Applied Energy 223 (2018) 369–382

Contents lists available at ScienceDirect

Applied Energy

journal homepage: www.elsevier.com/locate/apenergy

The use of strontium ferrite in chemical looping systems

Ewa Marek[a,b,*], Wenting Hu[a,c], Michael Gaultois[d,1], Clare P. Grey[d], Stuart A. Scott[a]

[a] Department of Engineering, University of Cambridge, Trumpington Street, Cambridge CB2 1PZ, United Kingdom
[b] Institute of Power Engineering, Augustowka 36, Warsaw 02-981, Poland
[c] School of Chemical Engineering and Advanced Materials, Newcastle University, Newcastle upon Tyne NE1 7RU, United Kingdom
[d] Department of Chemistry, University of Cambridge, Lensfield Road, Cambridge CB2 1EW, United Kingdom

HIGHLIGHTS

- Stable performance (conversion, particle durability) in fluidized bed tests over 30 redox cycles.
- Easily reduces below δ = 0.5; the final products of $SrFeO_{3-\delta}$ reduction are Fe and SrO.
- Attractive for CO or H_2 production; the reduced material regenerates in mild oxidizers (H_2O, CO_2).
- Catalytically assists with combustion of lean CH_4 (2.5%) in fluidized bed tests at T > 550°C.

GRAPHICAL ABSTRACT

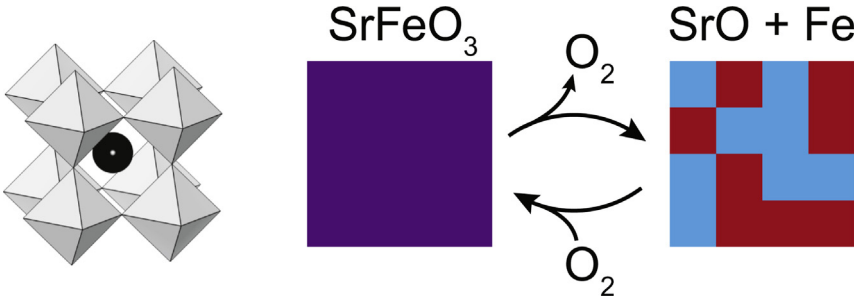

ARTICLE INFO

Keywords:
Chemical looping combustion
CLC
Hydrogen production
Perovskite
Strontium ferrite
Oxygen carrier

ABSTRACT

This work reports a detailed chemical looping investigation of strontium ferrite ($SrFeO_{3-\delta}$), a material with the perovskite structure type able to donate oxygen and stay in a nonstoichiometric form over a broad range of oxygen partial pressures, starting at temperatures as low as 250°C (reduction in CO, measured in TGA). $SrFeO_{3-\delta}$ is an economically attractive, simple, but remarkably stable material that can withstand repeated phase transitions during redox cycling. Mechanical mixing and calcination of iron oxide and strontium carbonate was evaluated as an effective way to obtain pure $SrFeO_{3-\delta}$. In–situ XRD was performed to analyse structure transformations during reduction and reoxidation. Our work reports that much deeper reduction, from $SrFeO_{3-\delta}$ to SrO and Fe, is reversible and results in oxygen release at a chemical potential suitable for hydrogen production. Thermogravimetric experiments with different gas compositions were applied to characterize the material and evaluate its available oxygen capacity. In both TGA and in-situ XRD experiments the material was reduced below δ = 0.5 followed by reoxidation either with CO_2 or air, to study phase segregation and reversibility of crystal structure transitions. As revealed by in-situ XRD, even deeply reduced material regenerates at 900°C to $SrFeO_{3-\delta}$ with a cubic structure. To investigate the catalytic behaviour of $SrFeO_{3-\delta}$ in methane combustion, experiments were performed in a fluidized bed rig. These showed $SrFeO_{3-\delta}$ donates O_2 into the gas phase but also assists with CH_4 combustion by supplying lattice oxygen. To test the material for combustion and hydrogen production, long cycling experiments in a fluidized bed rig were also performed. $SrFeO_{3-\delta}$ showed stability over 30 redox cycles, both in experiments with a 2-step oxidation performed in CO_2 followed by air, as well as a single step oxidation in CO_2 alone. Finally, the influence of CO/CO_2 mixtures on material performance was tested; a fast and deep

* Corresponding author at: Department of Engineering, University of Cambridge, Trumpington Street, Cambridge CB2 1PZ, United Kingdom.
E-mail address: ejm94@cam.ac.uk (E. Marek).
[1] Current address: Leverhulme Research Centre for Functional Materials Design, The Materials Innovation Factory, Department of Chemistry, University of Liverpool, 51 Oxford Road, Liverpool L7 3NY, United Kingdom.

https://doi.org/10.1016/j.apenergy.2018.04.090
Received 17 November 2017; Received in revised form 14 April 2018; Accepted 27 April 2018
Available online 03 May 2018

reduction in elevated p_{CO2} makes the material susceptible to carbonation, but the process can be reversed by increasing the temperature or lowering p_{CO2}.

1. Introduction

The concept of chemical looping (CL) utilises the reversible reduction and oxidation of suitable materials in many interesting processes. It was demonstrated that the reduction of metal oxides (Me_xO_y) can be employed in air-less combustion, where the oxygen needed for fuel conversion comes from the solid material instead of air:

$$(2\,n+\,m/2)Me_xO_y + C_nH_m \rightarrow (2\,n+\,m/2)Me_xO_{y-1} + nCO_2 + m/2H_2O \quad (1)$$

The reduced oxide can be then regenerated in a separate process, e.g. in air, closing the chemical loop:

$$Me_xO_{y-1} + 1/2O_2 \rightarrow Me_xO_y \quad (2)$$

Besides combustion, the chemical looping concept was also proposed for hydrogen production. It has been shown that for some reduced oxides even very mild oxidizers such as H_2O or CO_2 might be used [1], and a combustible gaseous product is generated: hydrogen or carbon monoxide respectively, i.e.

$$Me_xO_{y-1} + CO_2/H_2\,O \rightarrow Me_xO_y + CO/H_2 \quad (3)$$

Over the last 20 years, extensive research has been carried out to firstly investigate, then design materials that can work as oxygen carriers (OC), providing oxygen for the combustion application. Most of them involved oxides of transition metals, which in the suitable temperature range (500–800°C) exist as solid compounds in various oxidation states. Fe, Ti, Mn, Cu, Ni oxides as mono-metallic carriers and their mixtures as bi-metallic carriers were investigated extensively, in laboratory scale as well as pilot scale combustion experiments [2–5]. To improve the oxygen carrier's stability during the redox cycling, an addition of supporting component that is nominally inert (Al_2O_3 [6], ZrO_2 [7]) or active (CeO_2 [8]) is usually employed. Comprehensive reviews on metal oxides used for combustion are given by Imtiaz et al. [9] and Luo et al. [10], and for hydrogen production by Thursfield et al. [11] and Voitic and Hacker [12].

Ternary oxides with a perovskite structure AMO_3 (where A is commonly some alkaline earth or rare earth metal and M some transition metal), are also frequently considered for chemical looping applications. At elevated temperature and/or in reducing conditions some perovskites have been shown to maintain their crystal structure while gradually losing oxygen [13]:

$$AMO_3 \leftrightarrow AMO_{3-\delta} + \frac{\delta}{2}O_2 \quad (4)$$

The resulting $AMO_{3-\delta}$ structure is stable, containing M-cations with mixed valency and significant oxygen nonstoichiometry. Moreover, depending on the oxygen partial pressure, $p_{O2,}$ and temperature, T, the cubic perovskite structure $AMO_{3-\delta}$ may completely or partially convert to brownmillerite, an orthorhombic phase $AMO_{2.5+\delta}$ with some surplus oxygen. As a result either one of the nonstoichiometric structures or both may be detected during reduction [14,15].

Previous studies indicate that the kinetics of oxygen release from the perovskite structure (reaction (4)) are very fast under typical process conditions. Thus, when the oxygen release occurs, it often becomes limited by O_2 fugacity [16]. However, a partial substitution of A and/or M-site cations by metallic dopants with similar ionic size can alter the thermodynamic behaviour of the material in reaction (4) [17,18]. Perovskites have been proposed for use in many processes, such as carrier materials for oxygen production and storage applications [14,19,20], oxygen carriers in combustion and hydrogen production [17,21–23]; electrodes in solid oxide fuel cells [24,25]; as well as materials for selective ionic membranes in H_2 production [17,26] or CO_2 separation [27,28].

Potential materials with perovskite structures tested in chemical looping applications include $CaMnO_{3-\delta}$, $SrFeO_{3-\delta}$, $LaFeO_{3-\delta}$, $SrCoO_{3-\delta}$ [4,16,29,30] and multi-component materials with mixed metals for A or M cation sites, or for both sites, such as: $SrFe_{1-x}Cu_xO_{3-\delta}$, $SrFe_{1-x}Co_xO_{3-\delta}$ and $La_{1-x}Sr_xCo_{1-y}Fe_yO_{3-\delta}$ [14,20,31]. Similar materials, usually perovskites of Fe or Mn, were also investigated for hydrogen production: $La_{1-x}Sr_xFe_{1-y}Mn_yO_{3-\delta}$, $La_{1-x}Sr_xMnO_{3-\delta}$, $La_{1-x}Sr_xFeO_{3-\delta}$, $LaFeO_{3-\delta}$, $LaFe_xCo_yO_{3-\delta}$, $La_{1-x}Sr_xCo_{1-y}Fe_yO_{3-\delta}$ [17,32–36].

For chemical looping applications the main incentive in solid carrier selection will be its cost, inseparably linked to material's stability and abundance. One of the perovskite type compounds that may fulfil these requirements is $SrFeO_{3-\delta}$ as it does not contain expensive elements, such as rare (lanthanum) or toxic (cobalt) metals. Thus far, the strontium ferrite perovskite has been primarily considered for oxygen storage and air separation processes due to the low temperature at which the material starts losing oxygen, even at high p_{O2} (around 400°C in air) [14,29].

This study shows that $SrFeO_{3-\delta}$ is also attractive for two additional processes: hydrogen production and catalytic CH_4 combustion. Experiments in fluidized bed setup reveals that lean CH_4 (2.5%) combusts on $SrFeO_{3-\delta}$ at moderate temperatures > 550°C. The investigation also explores $SrFeO_{3-\delta}$ characteristics during high temperature reduction carried out in highly reducing atmospheres. The reversibility has also been studied here by oxidation either with air or with a mild oxidizer. This work reports that the reduction from $SrFeO_{3-\delta}$ to SrO and metallic Fe is remarkably reversible and results in oxygen release at a chemical potential suitable for hydrogen production, despite the severe changes in structure during the phase transition. The subsequent reoxidation, either in CO_2 or air, quickly regenerates the material from SrO and Fe back to a perovskite structure: $SrFeO_{2.5}$ in CO_2, or $SrFeO_{3-\delta}$ in air. Owing to reversibility of the reconstructive phase transition, the useful oxygen capacity is much higher than would be expected considering the maximum available by exploiting the $SrFeO_{3-\delta}$ phase alone.

2. Experimental

2.1. Materials preparation

Preliminary investigation used solid state synthesis by manual mixing of stoichiometric amount of Fe_2O_3 with either SrO or $SrCO_3$ (all > 98 wt%, Sigma Aldrich), using a mortar and a pestle until a mixture with homogenous appearance was obtained. The mixture was then calcined in a muffle furnace at 1000°C, for 3 h in air. Characterization of this material showed that the precursor $SrCO_3$ was much more effective in producing the desired $SrFeO_{3-\delta}$ phase.

In order to scale up the production of the perovskite for experiments in the fluidized bed rig, a planetary ball mill (MTI, model MSK-SFM-1) was used for powder mixing. Stoichiometric amounts of $SrCO_3$ (0.72 mol) and Fe_2O_3 (0.36 mol) were mixed in the ball mill for 3 h at 25 Hz. Ethanol (50 mL, 99.8%, Fisher Scientific) was added as a binder to improve mixing. The mixture was dried for 24 h at 50°C, and sieved to < 50 μm, 50–180 μm and 180–355 μm fractions. Then the particles were calcined in 1 to 4 stages, with each stage consisting of calcination at 1000°C for 3 h, followed by cooling to room temperature. As a result, four batches of material were prepared, differing in the total duration of calcination (between 3 and 12 h). All materials were sieved again after

final calcination. Unless stated otherwise, the $SrFeO_{3-\delta}$ sample used in the experiments was a sample taken from the large batch of material prepared with the ball mill.

2.2. Materials characterization

For phase identification of the synthesised and tested materials, X-ray powder diffraction (XRD) was performed using a PANalytical Empyrean diffractometer. Rietveld or Pawley refinement was performed using the Topas Academic V4 software [37]. Starting structures of phases used were Fe (ICSD 53452), Fe_2O_3 (ICSD 15840), SrO (ICSD 109461), $SrCO_3$ (ICSD 15195), $Sr_3Fe_2O_7$ (ICSD 74422), $SrFe_{12}O_{19}$ (ICSD 69022), $SrFeO_{2.5}$ (ICSD 91065), and $SrFeO_3$ (ICSD 91062). Accounting for the nonstoichiometric and lower-symmetry perovskite phases of $SrFeO_{2.75}$ and $SrFeO_{2.875}$ did not improve the quality of the fit, therefore the compositions are reported with the best fit obtained using cubic $SrFeO_3$.

A typical diffractogram was collected in the range of 2θ from 5° to 80° using Cu Kα radiation with a voltage of 40 kV and current 40 mA. To investigate possible $SrFeO_{3-\delta}$ transformations and the final products of long $SrFeO_{3-\delta}$ reduction, in-situ X-ray powder diffraction was performed using an Anton-Paar XRK 900 furnace, with a total gas flow rate of 1.0L/min. Temperature induced reduction and reoxidation were carried out in 5% H_2/N_2 and air, at temperatures from 25°C up to 900°C.

An additional in-situ experiment was performed to analyse possible reoxidation with CO_2. Here, the program included temperature induced reduction (similar to temperature programmed reduction, TPR, in TGA, 2.3) carried out from room temperature to 900°C in 5% H_2/N_2, continued for additional 1.5 h at 900°C, followed by long isothermal reoxidation with CO_2 at 900°C (130 min), then reoxidation in air at 900°C. During temperature ramp the sample was heated up to an intermediate temperature (100, 400, 600, 800, 850°C with 50°C/min heating rate), where X-ray scans lasting between 5 and 17 min were performed, then the sample was heated up to the next temperature and the procedure was repeated. The total time for all the heating steps, including duration of the isothermal intervals for the X-ray scans gave was the same as the duration of TGA-TPR tests, performed with temperature ramp rate of 10°C/min.

2.3. TGA experiments

Thermogravimetric analysis (TGA) was used to characterize basic thermochemical properties of the $SrFeO_{3-\delta}$ perovskite. TGA experiments were carried out in a TGA/DSC 1, Mettler Toledo analyser with a horizontal reaction chamber. A balance arm was located in the middle of the chamber, upon where an alumina crucible containing a test sample was placed. Throughout the experiments, the chamber was purged with protective and purge gas flows (50 mL/min each, measured at 20°C and 1 bar, as were all gas flows quoted hereafter), usually Ar and in one case Air (to obtain $p_{O2} = 0.21$ bar). A reactive gas was supplied through a capillary tube located above the crucible. The reactive gas was chosen as needed in an experiment, keeping a constant gas flow of 50 mL/min. The following gases were supplied through the capillary: Ar, Air, N_2, 5% CH_4/N_2, 5% H_2/N_2, 10% CO/N_2, 20% CO_2/N_2, (all BOC, > 99.99%, compositions of mixtures were specified on a mole basis). For gases supplied through the capillary, the concentration is about three times lower at the sample due to the dilution with the protective and purge gases. Around 20–50 mg of $SrFeO_3$ was used in each experiment, with particle size < 50 μm.

Two types of TGA experiments were performed. The first was a temperature programmed reduction and oxidation (TPR/TPO), in which a sample was held in a constant atmosphere and its temperature was first increased to a target value at a constant rate (5–15°C/min), followed by a decrease at the same rate, with the option to switch the atmosphere during cooling. This procedure was repeated several times on a sample to test the material's stability over a few redox cycles. The second type of experiments involved sample being heated up to a demanded temperature between 400 and 900°C, followed by an isothermal step, where the sample was kept for 2–3 h. During the isothermal step, different reactive gases could be used sequentially. If needed, the isothermal step was repeated at different temperatures.

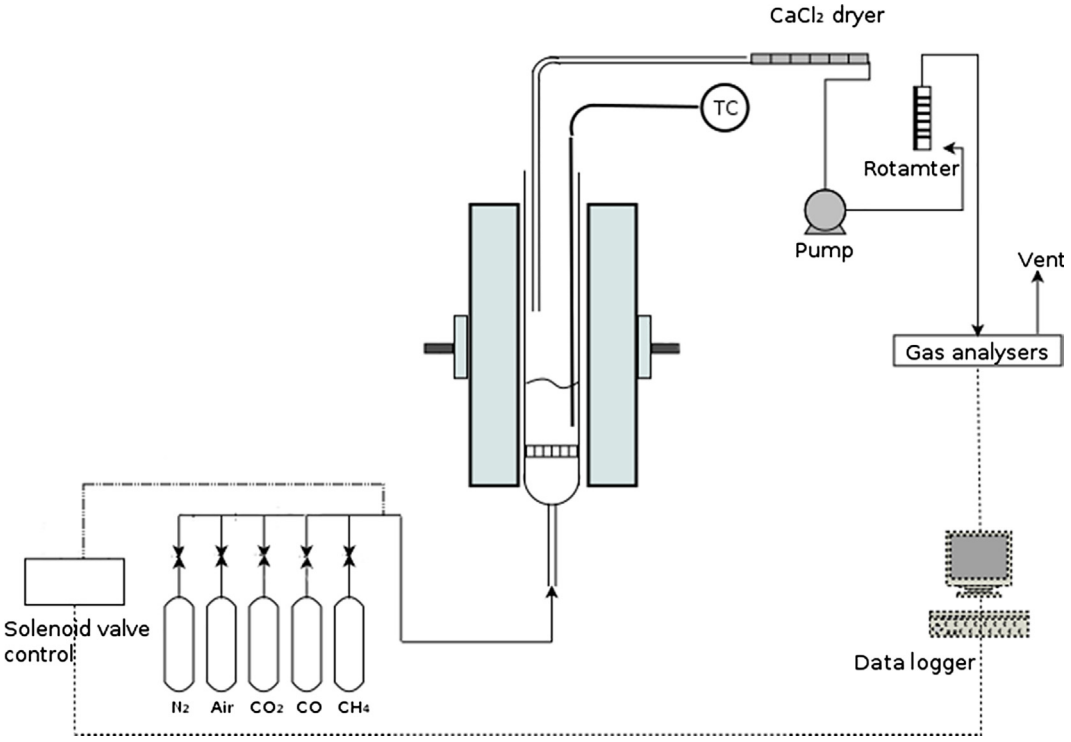

Fig. 1. Experimental setup with small scale fluidized bed reactor (i.d. 25 mm).

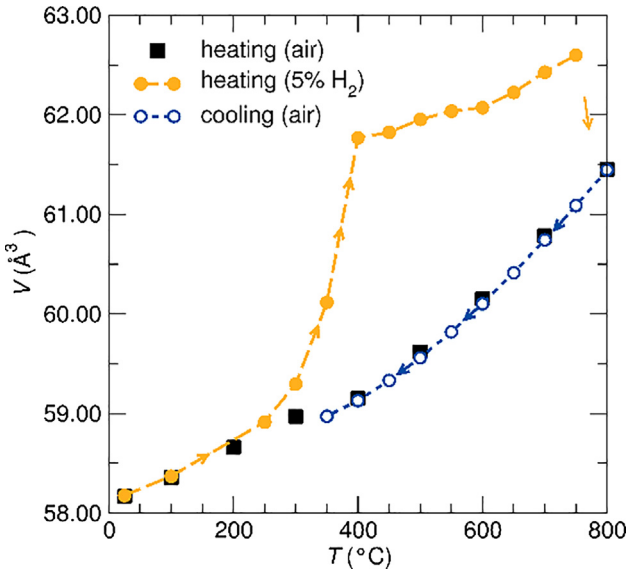

Fig. 3. Material composition determined from Rietveld refinement of XRD patterns collected during reduction of $SrFeO_{3-\delta}$ in 5% H_2 (95% N_2). Data was collected under isothermal conditions at discrete temperatures from 25 to 900°C. At 800°C under 5% H_2, cubic $SrFeO_{3-\delta}$ begins to decompose, and by 900°C decomposes completely to form SrO and Fe. Cubic $SrFeO_{3-\delta}$ is completely regenerated in < 1 min when exposed to air.

2.4. Fluidized bed experiments

A fluidized bed reactor was used to investigate material's behaviour during multistep redox cycling. Fig. 1 presents a schematic representation of the reactor system. The bed was held in a quartz reactor, equipped with a porous disc: a gas distributor, located 110 mm from the gas inlet. The reactor was electrically heated with a tubular furnace to a demanded experimental temperature, here up to 850°C. From the top of the reactor a K-type thermocouple was inserted to allow for temperature control, measuring the temperature of the bed material ~1 cm above the porous disk. Gas flows, provided from the bottom of reactor, were controlled with a system of solenoid valves and rotameters. At the top of the reactor a sampling tube was inserted in order to continuously sample the outlet gas for the composition measurements. The sample gas flow was induced with a pump (16 mL/s) and directed through a drying tube (filled with $CaCl_2$) to a gas analyser (ABB EL3020) for O_2, CH_4, CO and CO_2 measurement.

CH_4 combustion experiments were carried out between 400 and 700°C, using 15 g of $SrFeO_{3-\delta}$, 150–355 µm, as a bed material. The reactor was heated up to the temperature set-point in the flow of air, after which the gas was switched to nitrogen for 15 s. Then the flow was switched to 2.5% CH_4/N_2 (created with 5% CH_4/N_2 and N_2) to investigate methane combustion. In between experiments, the bed material was reoxidized in air for a minimum of 5 min or until a stable 20.8% oxygen concentration at the reactor outlet was measured, whichever was longer.

Cycling experiments with either two or three-step redox procedure were performed in the fluidized bed reactor using SiO_2 as the bed material (David Ball Group, washed and dried, 250–355 µm, 15 cm^3 unfluidized). The temperature was kept at 850°C with a constant gas flow of 32 mL s^{-1} (U/U_{mf} ~10). A 10% CO/N_2 or 5% CO/10% CO_2/N_2 mixture was used as the reducing agent for 8 min during the reduction stage. For the two-step procedure, oxidation was performed with 20% CO_2/N_2 mixture for 5 min; and for the three-step procedure, the oxidation involved 5 min with 20% CO_2/N_2 and a further 5 min with air. Between each gas switch the reactor was purged with N_2 for 0.5 min. A single experiment consisted of 31 cycles, where the first cycle was a blank, after which $SrFeO_{3-\delta}$ sample (0.75 g) was dropped-into the reactor (during the reduction stage) and the required redox cycles were performed.

To check the durability of the particles, the material was quenched and recovered after the last oxidation cycle in experiment with 10% CO/N_2 for reduction and a 2-step oxidation. The reactor was rotated by 180° and the bed material slipped into a quartz Schlenk flask, where it cooled quickly to room temperature in the flow of air. The $SrFeO_{3-\delta}$ sample was then separated from SiO_2 with magnet and sieves.

3. Results

3.1. Phase identification

Regardless of the Sr precursor used in solid synthesis, both prepared Sr-Fe mixtures were black in colour after calcination. The XRD patterns and detailed composition of the materials determined by Rietveld refinement are provided in the supplementary material (ESI S.1 and ESI S.Table1). XRD revealed the material produced from SrO and Fe_2O_3 contained a mixture of Fe_2O_3, $SrFe_{12}O_{19}$, $Sr_3Fe_2O_7$, and $SrFeO_{3-\delta}$, whereas material produced from $SrCO_3$ yielded > 90 wt% $SrFeO_{3-\delta}$ after a single calcination step at 1000°C for 3 h (cf. ~40 wt% $SrFeO_{3-\delta}$ for the same treatment when starting from SrO). As indicated in Section 2.1, ball milling was used as a mixing technique for preparation of larger batches of $SrFeO_{3-\delta}$. The milling itself did not result in any detectable solid state reaction as only Fe_2O_3 and $SrCO_3$ were detected in the milled sample, with the composition obtained in the refinement close to that of the starting materials (obtained: 36.0 ± 0.3 wt% Fe_2O_3 and 64.0 ± 0.3 wt% $SrCO_3$; expected: 35.1 wt% Fe_2O_3 and 64.9 wt% $SrCO_3$). The sample after calcination had a very well developed microstructure, as can be seen in the SEM picture (ESI S.2).

In comparison to other synthesis methods used in solid carrier preparation for chemical looping applications, mechanical mixing and calcination can be easily scaled up. Solid state synthesis has been broadly used in $SrFeO_{3-\delta}$ studies [38–44] but the purity of the perovskite phase is not always reported. In contrast, the work of Lau et al. [29] indicates that wet synthesis methods (nitrates and Pechini) resulted in a mixture containing only 68 wt% of the $SrFeO_{3-\delta}$ perovskite, among other Sr-Fe-O compounds. The results given in ESI S.Table 1 indicate that mechanical mixing of inexpensive Fe_2O_3 and $SrCO_3$ powders followed by calcination is effective, and leads to nearly phase-pure material; more than 2 calcination steps do not appear to lead to further changes in phases. Interestingly, only the mixture prepared with SrO and Fe_2O_3 resulted in the brownmillerite, $SrFeO_{2.5}$ phase.

3.2. In-situ XRD analysis

In-situ XRD was performed during high temperature reduction and oxidation to monitor changes in the $SrFeO_{3-\delta}$ structure during these processes. Fig. 2 presents results from cell volume calculations during temperature treatment between room temperature and 800°C. When the material was heated under 5% H_2 the perovskite unit cell volume diverges from values obtained in air above 300°C, indicating activity and higher oxygen nonstoichiometry. The largest divergence is seen between 350°C and 400°C. Upon exposure to air, the cell volume contracts to values indistinguishable from untreated sample. The indistinguishable unit cell volume suggests good reversibility and quick equilibration of this process. The unit cell volumes observed here agree with unit cell volumes observed by Taylor et al. [45] during exposure to CH_4 and air, although the reduction with CH_4 started above 450°C, a higher temperature than observed here in 5% H_2.

In the prolonged reduction under 5% H_2 with increasing temperature performed here, $SrFeO_{3-\delta}$ started decomposing into SrO and Fe at 800°C. Fig. 3 shows the change in the sample composition determined by Rietveld refinement of XRD patterns collected isothermally at discrete temperatures. The presence of metallic iron is seen before SrO. This could be due to the formation of phases that diffract weakly and

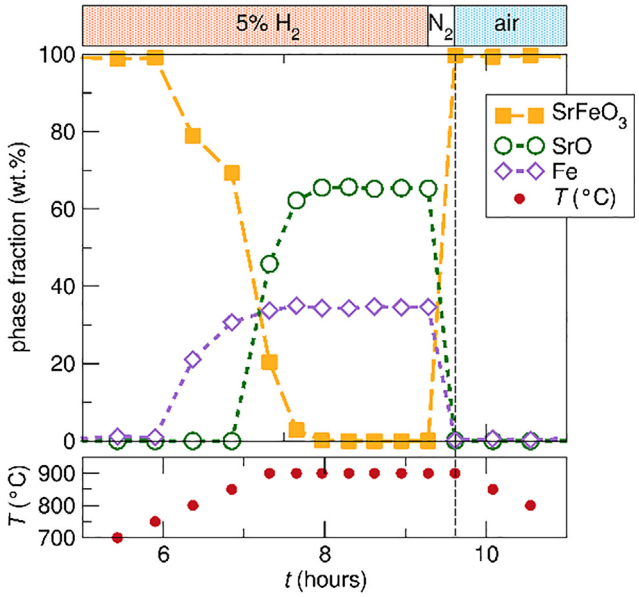

Fig. 2. The unit cell volume of $SrFeO_{3-\delta}$ determined by Rietveld refinement of in-situ XRD patterns collected isothermally in air, or during reduction in 5% H_2 and reoxidation in air. When heated under 5% H_2 the unit cell volume diverges at 300°C, consistent with the onset of reduction and higher oxygen non-stoichiometry. Upon exposure to air, reoxidation is rapid and the unit cell volume is indistinguishable from a sample that has not been reduced under 5% H_2.

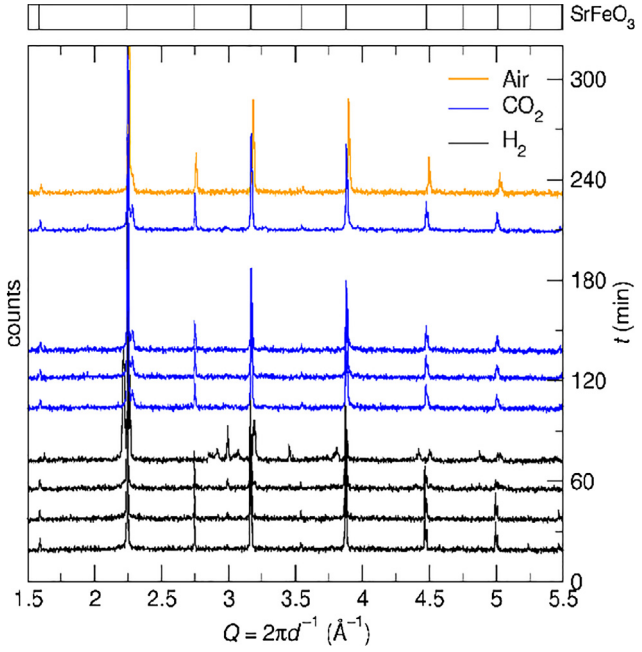

Fig. 4. In-situ XRD patterns obtained at 900°C, during reduction in 5% H_2, followed by reoxidation in CO_2 and then air. Prolonged reduction results in decomposition of cubic $SrFeO_{3-\delta}$; introducing CO_2 regenerates the original cubic $SrFeO_{3-\delta}$, and exposure to air reoxidizes the sample further.

thus are not observed. This most likely corresponds to Sr-rich intermediate phases, which may be less crystalline, and would have lower symmetry and thus less intense peaks. As reported in the literature, reduction of oxygen depleted strontium ferrite, $SrFeO_{2.5}$, results in the formation of metallic iron and homologous series $Sr_{n+1}Fe_nO_{3n+1}$ of layered perovskite structures in Ruddlesden–Popper (RP) phases [40,42]. $Sr_2FeO_{4-\delta}$ (n = 1) and $Sr_4Fe_3O_{10-\delta}$ (n = 3) phases are considered unstable at high temperatures, reducing to $Sr_3Fe_2O_{7-\delta}$ (n = 2) [46]. Additionally, $SrFeO_{3-\delta}$ can also tolerate deviations from cation stoichiometry, both on Sr- and Fe-deficient sites, which in turn allows for $SrFeO_{3-\delta}$ to coexist with RP phases or other Sr-Fe-oxides, $SrFe_{12}O_{19}$ or $Sr_4Fe_6O_{13}$ [46,47]. Nevertheless, no RP phases nor other Sr-Fe-oxides were visible in the in-situ diffraction patterns, likely owing to the low phase fraction present, if at all. Still, it is important to note that not all reflections in the diffraction patterns were accounted for by the refinement (see ESI S.3), even when material was reduced to 35 wt% Fe and 65 wt% SrO (as expected from stoichiometry for full reduction). Following the reduction and purging with nitrogen, reoxidation in air occurs rapidly, and reforms the cubic $SrFeO_{3-\delta}$ perovskite in < 5 min (Fig. 3 and ESI S.3).

During heating, $SrFeO_{3-\delta}$ loses oxygen and results in the distortion and transformation of the crystal structure [15]. Depending on the nonstochiometry, $SrFeO_{3-\delta}$ at room temperature has a tetragonal, orthorhombic or mixed structure [43,46,48], that, with increasing temperature, transforms into a cubic form (266°C [46]). Under low p_{O2} cubic $SrFeO_{3-\delta}$ transforms to orthorhombic structure (> 535°C [45]), before forming back a cubic structure (~835°C [45]). Similarly, Mizasuki et al. who investigated the phase transitions during deep $SrFeO_{3-\delta}$ reduction (with H_2), concluded that material transitions from a cubic perovskite to a mixed perovskite ($SrFeO_{3-\delta}$)-brownmillerite ($SrFeO_{2.5+\delta}$) structure and returns back to the cubic geometry at 900°C [15]. Grenier et al. showed that orthorhombic brownmillerite ($SrFeO_{2.5+\delta}$) transitions to a cubic perovskite-like structure, and the process depends on temperature and p_{O2} but should be completed above 850°C [39]. Since the temperatures of Sr-Fe-O phase transitions depend on p_{O2}, some differences between reported results are expected.

In this study, however, the fresh and in-situ analysed samples appeared to only have the cubic structure of $SrFeO_{3-\delta}$. More detailed studies (i.e. [45]) have previously been carried out using neutron diffraction to carefully and systematically determine the structural transitions of the Sr-Fe-O phases. With this in mind, refinements were attempted using other orthorhombic or tetragonal spacegroups, though the quality of the fit was not improved. This lack of sensitivity may be due in part to the use of X-rays in this study, which are less sensitive to the ordering of oxygen atoms.

During the second in-situ experiment material was reoxidized firstly in CO_2, similarly to the experiment performed in TGA (2.3). Fig. 4 shows selected XRD patterns collected during the experiment at 900°C under 5% H_2, which show evidence for continued reduction and phase segregation. Cubic $SrFeO_3$ is the primary phase for ~60 min, though by 80 min there is no longer any $SrFeO_3$ present. After ~60 min at 900°C under 5% H_2, $SrFeO_3$ decomposes into a mixture of Fe and a complex phase mixture that could not be well described.

When the gas was switched to CO_2 a very fast reoxidation was observed, and cubic $SrFeO_3$ was regenerated as a single phase. The prolonged exposure to CO_2 afterwards did not seem to influence the material's structure significantly. When air was introduced in the final step the material reoxidized completely, as tracked by changes in the peak positions as the unit cell volume decreases with higher O-content. No carbonation was detected during reoxidation with CO_2. The experiment was also repeated at 800 and 850°C, however at these temperatures no phase separation to Fe and Sr-Fe-oxides was observed. Again, no carbonation was detected at both lower temperatures after CO_2 reoxidation.

3.3. TGA analysis

3.3.1. Oxygen uncoupling in air

The capability of the strontium ferrite to reversibly change its oxygen vacancy was also investigated with temperature programmed reaction in air (used both as protective and reactive gas in the TGA). The temperature of the sample was changed from 50°C to 900°C and back to give a preliminary assessment of the rates of the reaction. To

test the influence from phase impurities on O_2-uncoupling behaviour, two samples prepared by manual mixing were examined: after 1 calcination (highest share of impurities: 9.0(± 3.0) wt% $Sr_3Fe_2O_7$) and after 4 calcinations (smallest load of impure phases: 3.0(± 0.4) wt% $Sr_3Fe_2O_7$).

The reversibility of the oxygen release can be seen for the sample of $SrFeO_{3-\delta}$ after 1 calcination (3 h) in Fig. 5, where it was subjected to 8 cycles of heating and cooling between 50 and 900°C at a heating rate of 10°C/min. Apart from the first cycle, the behaviour of the material was stable, although the number of cycles was limited. As noticed by Lau et al. [29] $SrFeO_{3-\delta}$ and other Sr-Fe-O components are susceptible to CO_2 absorption at low temperature, noticeable even during sample storage (although not detected in XRD analysis, see ESI S.Table 1). This explains the observed difference in the sample mass loss between first cycle and all consecutive cycles of the TPR/TPO program (Fig. 5). To avoid this behaviour the procedure suggested by Lau et al. [29] was performed, i.e. a decarbonation cycle (TPR/TPO in air, 10°C/min) immediately prior to each TGA experiment described later. The presence of carbonates in the stored samples was also confirmed during experiments in fluidized bed (ESI S.12).

The overlap of sample mass during the heat-ups (reduction) and cool-downs (oxidation) in Fig. 5 indicates that the observed reversible reaction was limited by equilibrium rather than kinetics. This was confirmed further by the invariant mass-temperature relationship when the experiment was repeated with different heating rates (5, 10 and 15°C /min), shown in supplementary material (ESI S.9). Thus it suggests that the kinetics of the reaction is fast.

Another interesting feature is the hysteresis observed between 700 and 800°C. It is likely that this feature is due to a different reaction in this temperature range, perhaps owing to the presence of an impurity phase. If the hysteresis was caused by the presence of impurities, it would be expected that the material calcined for 3 h would exhibit more significant hysteresis than the material calcined for 12 h, as the latter had higher share of $SrFeO_{3-\delta}$ (ESI S.Table 1). Indeed, when the two samples are compared (Fig. 6), the sample of higher purity shows less hysteresis. Similarly, no hysteresis was observed for 12 h-calcinated sample mixed in the ball mill.

3.3.2. Oxygen release in other atmospheres

Oxygen release experiments were also conducted using, as the reactive gas, Air, N_2, CO_2 or H_2 for the reduction stage (TPR) and air or CO_2 for the reoxidation (TPO). In these experiments, Ar was used as the protective gas, therefore the effective concentrations above the sample were lower owing to gas mixing in the TGA, i.e. during oxidation p_{CO2} and p_{O2} were ~0.07 bar. Results from the TPR and TPO of $SrFeO_{3-\delta}$ are presented in Fig. 7. It can be seen that both the starting point and the rate of oxygen release depend on the reactive gas used. Not surprisingly oxygen release in H_2 starts at the lowest temperature (among the curves shown in Fig. 7A) and is the fastest. It can be assumed that hydrogen reacts with lattice oxygen on the sample surface and/or combusts with oxygen released from the sample to the gas phase. Both mechanisms are possible but the difference between starting temperatures for reduction in H_2 (340°C) and inert N_2 (370°C) (see a zoom into Fig. 7A in ESI S.10) suggests a surface reaction.

Interestingly the $SrFeO_{3-\delta}$ reduction started at lower temperature when air was used in the experiment (p_{O2} = 0.07 bar) rather when CO_2 (p_{CO2} = 0.07 bar) was applied. Similar effects of CO_2 were noted by Lau et al. [29] for oxygen release by $SrFeO_{3-\delta}$ and Bucher et al. [49] for $Ba_{0.5}Sr_{0.5}Co_{0.8}Fe_{0.2}O_{3-\delta}$, and were explained by the adsorption of CO_2 on the surface, which inhibits the release of O_2.

Reoxidation of the sample with air (Fig. 7C) followed the same path as the reduction. For samples reduced in other atmospheres, the reoxidation was very fast initially and was largely identical to the sample reduced in air thereafter, no matter how deeply the sample was reduced at the end of the TPR. This observation suggests again that the kinetics of the oxidation of the materials can be extremely fast away from chemical equilibrium.

Reduction in hydrogen showed two distinctive stages. The first one lasted until the relative mass reached 0.973. Such a large mass loss was never reached in inert or mildly oxidizing gas (relative mass ~0.980 at 900°C both in N_2 and CO_2), even when sample was held at high temperature for a prolonged time (see ESI S.11). This change observed between first and second stage of reaction probably indicates a transitional point, where material was reduced to $\delta = 0.5$ and where the perovskite-brownmillerite structural change has been completed.

The second stage of reduction (below 0.973 of relative mass) in combustible gas was at first slow, suggesting that stripping of O_2 from the solid was more difficult, however later the reduction accelerated as the TPR progressed and the temperature increased. Further reduction was also investigated after the TPR with an additional isothermal step, carried out for 1.5 h at 900°C as shown in Fig. 8. The sample never reached equilibrium and the final relative mass was 0.956. Despite the severe reduction in H_2, the transition was found to be completely reversible as the sample was reoxidized to the initial mass in the usual TPO program. Reoxidation to $SrFeO_{3-\delta}$ was also confirmed with XRD of the sample after the described TGA treatment (ESI S.4).

In this study, the total mass loss of 4.4% observed in the TPR and isothermal reduction in H_2, as shown in Fig. 8, must have been connected with the phase transitions and reduction from the perovskite structure to brownmillerite and further. The theoretical mass loss associated with O_2 release in $SrFeO_3$ to $SrFeO_{2.5}$ reduction can only be responsible for up to 4.18% of the mass loss. The starting perovskite shows some degree of oxygen nonstoichiometry, δ ($SrFeO_{3-\delta}$), so the amount of oxygen associated with the transition to brownmillerite is much less than 4.18%. Destruction of brownmillerite $SrFeO_{2.5}$ as suggested by the mass loss from TGA experiments is in agreement with observation from in-situ XRD H_2-reduction (3.2), where we observed diffraction patterns consistent with complete destruction and conversion of $SrFeO_{2.5}$ to Fe and SrO (Fig. 3).

To check products of the reduction in H_2, two samples for ex-situ XRD analysis were prepared in the TGA. The first sample was prepared by running TPR from 50 to 900°C then back to 50°C, all in the flow of H_2. The second sample was prepared in a program with 50–900°C TPR-

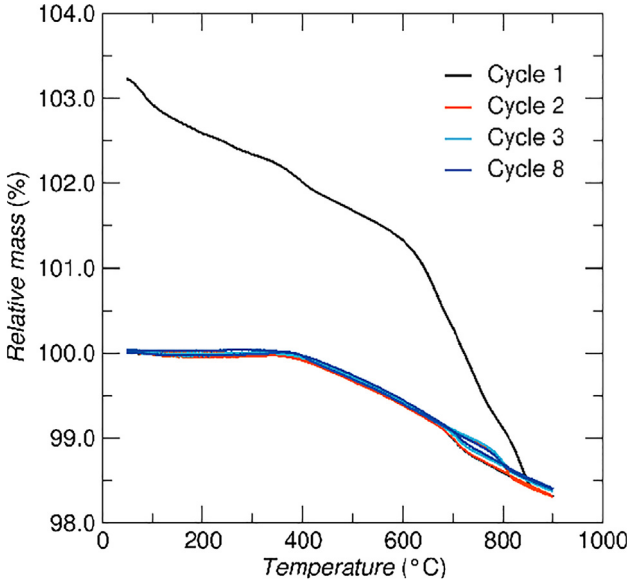

Fig. 5. TPR/TPO curves of $SrFeO_{3-\delta}$ in air (p_{O2} = 0.21 bar). Sample from a batch mixed manually and calcined for 3 h (1 calcination), subjected to 8 consecutive cycles of temperature program with a heating rate of 10°C/min. The first cycle starts with relative mass above 100% because the sample is partly carbonated, after exposure to air. The carbonates are decomposed on heating, therefore 100% mass corresponds to the decarbonated and oxidized state.

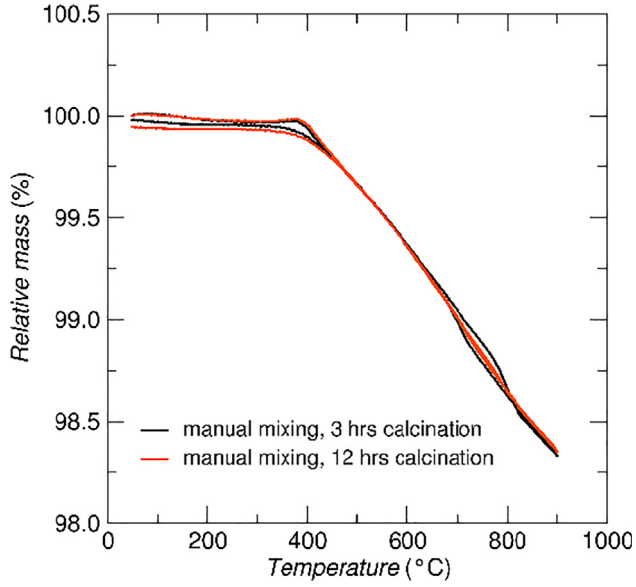

Fig. 6. TPR/TPO curves for $SrFeO_{3-\delta}$ in air (p_{O2} = 0.21 bar). Sample from a batch mixed manually and calcined for 3 h (1 calcination) or 12 h (4 calcinations). 5th cycle of temperature program with a heating rate of 15°C/min.

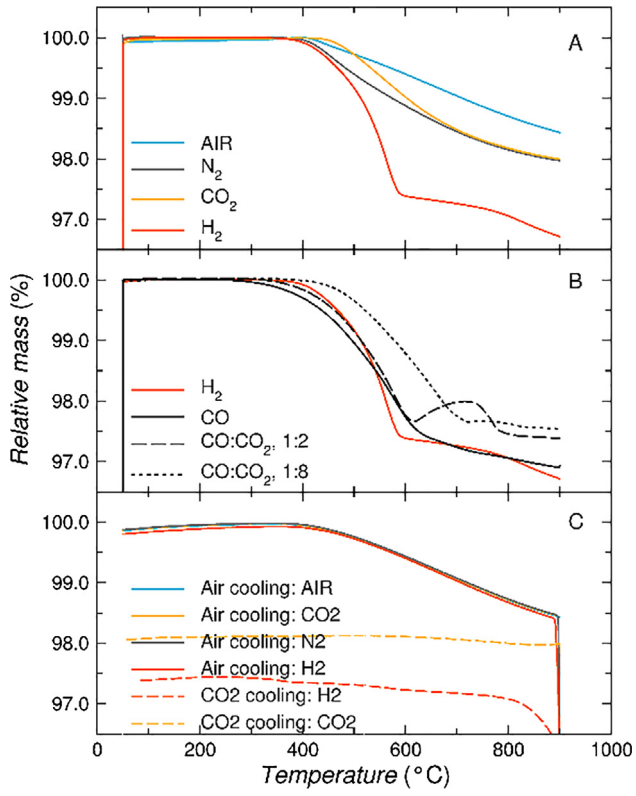

Fig. 7. Sample mass change during: (A) and (B) heat up: TPR program in various atmospheres; (C) cool down: TPO program in air or CO_2 (p_{O2} or p_{CO2} ~0.07), after reduction with different gases. Temperature change rate was 10°C/min.

H_2 stage, followed by 10 h of isothermal reduction at 900°C, then the sample was cooled to 50°C in the constant flow of H_2. In both cases, ex-situ XRD performed afterwards revealed the material did not reach equilibrium (i.e. reduction was not complete). The XRD pattern of the sample reduced for a longer time (10 h) (see ESI S.7) confirmed partial destruction of brownmillerite and formation of $Sr_3Fe_2O_7$, a Ruddlesden-Popper phase, as well as metallic iron along with brownmillerite

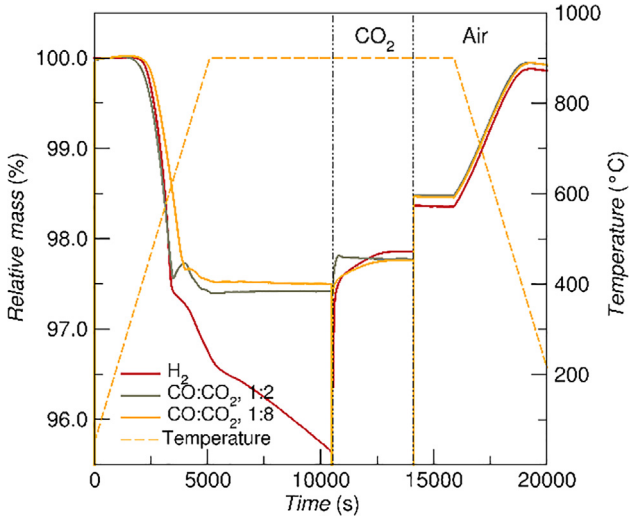

Fig. 8. Sample mass change during TPR-TPO program with an isothermal step at 900°C, carried out for 3 h: 1.5 h in a reducing atmosphere, then 1 h in 20% CO_2 and 0.5 h in air. Temperature change rate was 10°C/min.

$SrFeO_{2.5}$.

On the other hand, the XRD pattern of the first sample was dominated by $SrFeO_{2.5}$, accompanied by several reflections from an unidentified secondary phase (see ESI S.6), suggesting only a small amount of the brownmillerite was reduced. The secondary phase was not present in large enough amount to be identified, but in light of the phases present in the sample reduced for longer times, was likely $Sr_3Fe_2O_7$.

If taking the 0.973 value observed in reduction with H_2 as the phase transition boundary (with a stoichiometry $SrFeO_{2.5}$), then the synthesised perovskite can accommodate oxygen in the amount equal to 2.7% of its original mass. Therefore the average stoichiometry of product after calcination was $SrFeO_{2.82}$. This conclusion is in agreement with stoichiometry evaluations for samples prepared with a slow cooling step in air, where the compositions were reported to be in the range $SrFeO_{2.80}$-$SrFeO_{2.85}$ [15,43,44].

The sample after reduction in H_2 was also reoxidized in CO_2 (Fig. 8), which brought it back to a relative mass above that expected for $SrFeO_{2.5}$ (0.978 vs 0.973). Starkov et al. [42] suggested that the high temperature (900°C), low p_{O2} transition from brownmillerite to cubic perovskite is morphotropic and involves a change in chemical composition (i.e. it will not happen without oxygen incorporation to the orthorhombic structure). From their phase diagram, the material's cubic stoichiometry at 900°C would be $SrFeO_{2.52}$ which is in agreement with the final mass obtained in this study, when the reduced sample was reoxidized in CO_2 (0.978) [42]. Moreover, the isothermal reoxidation with CO_2 was fast until 0.973 of the starting mass was reached but then significantly slowed down and reached a plateau at 0.978. This mass change is also close to the final mass obtained when the 'as synthesised' sample was reduced with CO_2 (0.980) or with N_2 (0.978) (see ESI S.11), indicating that $SrFeO_{2.52}$ could be the stable phase in this conditions. XRD analysis of the sample reoxidized in CO_2 and cooled down in that atmosphere showed the presence of $SrFeO_{2.5}$, and no carbonation was observed (ESI S.5).

As seen in the TPO stage (Fig. 7C), CO_2 did not reoxidize $SrFeO_{3-\delta}$ following TPR in CO_2 and only partially reoxidized the sample after deep reduction in H_2. Air was needed to fully regenerate either of samples. Therefore it seems that the sample can be effectively reoxidized with CO_2 only if it was reduced firstly below the $SrFeO_{2.5}$ phase equilibrium point. In an experiment with a long isothermal step at 900°C in CO_2 (as shown in ESI S.11), a stable mass was reached, indicating equilibrium like conditions, similarly to the one observed in air. Such equilibrium was not met in H_2 TPR experiments (Fig. 8).

Fig. 7 B compares the reduction in H_2 with reduction in CO and CO/

CO_2 atmospheres. It can be noticed that the reduction with CO is fast and starts at a low temperature: 250°C in 10% CO and 325°C in 5% CO/10% CO_2, again below the temperature of spontaneous O_2 release seen in the inert atmosphere (N_2). This characteristic can make the material an attractive option for CO removal in applications such as exhaust gas cleaning (afterburning) or carbon striping in chemical looping. It is worth noticing that the mass increase after fast reduction in both CO/CO_2 mixtures most probably indicates carbonation. This small mass gain was lost quickly as temperature increased. Long isothermal reduction was also tested in a CO/CO_2 atmosphere (Fig. 8), and it was observed that the presence of CO_2 stops the material's reduction at a relative mass of about 0.975–0.976, and the process did not proceed even when temperature was ramped to 900°C. Therefore $p_{O2} \sim 10^{-16}$ bar (equivalent to $CO/CO_2 = 1:2$ at 900°C) was not sufficient to reduce the material to iron and RP phases. The slower conversion in CO/CO_2 with 1:8 ratio was not accompanied with as severe carbonation as was observed during TPR in CO/CO_2 with 1:2 ratio. After reduction, it was still possible to partially regenerate the material with CO_2 and later reoxidize it fully with air.

Reoxidation with CO_2 was tested further in an isothermal experiment in TGA at 850°C. The sample was reduced in H_2 oxidized with CO_2 and again reduced in H_2. As shown in Fig. 9, the regeneration with CO_2 was not sufficient to fully reoxidize the material. Nevertheless, the similar extent of reduction in H_2 and same oxidation level in CO_2 cycles indicate that $SrFeO_{3-\delta}$ may keep good durability even when cycled with partial CO_2-reoxidation only. The observed characteristic reveals the material's potential for hydrogen production (when H_2O is used in place of CO_2), similarly to lanthanum-containing perovskites ($La_xSr_yFeO_{3-\delta}$ and $La_xSr_yMnO_{3-\delta}$ – both tested without air oxidation [17,22,32], $LaFeO_{3-\delta}$ – 2 step oxidation [34], $LaFe_xCo_{y3-\delta}$ – 2 step oxidation [35]). To examine this further, cycling experiments with and without air oxidation step were also performed (see Section 3.4) and in both cases a stable $SrFeO_{3-\delta}$ performance for 30 cycles was observed.

3.3.3. Isothermal experiments in various atmospheres

In order to investigate the influence of the reduction potential on the nonstoichiometry of $SrFeO_{3-\delta}$, a set of isothermal experiments was also carried out in the TGA. In the first experiment, sample was heated up to 400°C in air, and kept in that atmosphere for 10–20 min until a stable mass was reached. Then atmosphere was changed to N_2 for 45 min, followed by a change to CH_4 for another 45 min. After reduction steps were finished, air was introduced for 10–20 min to reoxidize the sample. Then the temperature was increased by 100°C in air flow (which was accompanied with some mass change due to thermally-induced O_2 release), and the isothermal step was repeated. The second isothermal experiment was very similar, except that air was also introduced for 20 min in-between intervals of N_2 and CH_4 flow. In all of these experiments Ar was used as the protective gas, while the reactive gas was switched as needed. Therefore air flow resulted in $p_{O2} = 0.07$ bar, while CH_4 mixture flow gave $p_{CH4} = \sim 0.02$ bar.

Fig. 10A and B show that at 400°C reduction in CH_4 and N_2 was very similar, indicating that CH_4 behaved like an inert. From 500°C much faster reduction was observed in CH_4 than in N_2. At 600°C and above, the mass loss in CH_4 was so fast, that curves from two experiments were overlapping. In the case where the sample was oxidized prior to reduction by CH_4, the additional oxygen gained by the material was lost within 42–200 s at 600°C and above, indicating very fast reduction kinetics, and further reduction profiles were largely identical for both experiments. Furthermore, both samples reoxidized to the same mass each isothermal step started with. As shown in Fig. 11 the relative sample mass plotted against experimental temperature followed a straight line, and overlapped with that measured during the temperature programmed reduction in air. This is an important observation indicating that $SrFeO_{3-\delta}$ can withstand a severe multi-step reduction with ability of material re-oxidation without any noticeable difference in its quality before and after the redox experiment. Despite repeated phase transitions between perovskites and brownmillerite structures, the reduction to and below the brownmillerite phase seemed to be completely reversible.

3.4. Fluidized bed experiments

3.4.1. CH_4 combustion

Short experiments in the fluidized bed rig were performed in order to investigate the combustion of methane with $SrFeO_{3-\delta}$. Using model fuels like CO or H_2 for laboratory investigations may give an unfair picture of reactivity, particularly if the interest is the use of natural gas, rather than syngas. It has been shown that CH_4 can be difficult to combust, especially at low temperatures and in fluidized beds. Previous studies report that combustion of CH_4 can be observed above the bed at temperatures higher than 700°C and within the bed at temperatures above 900°C [50]. This is usually explained by the bed material promoting radical destruction and recombination, resulting in chemical quenching of the gas phase combustion. With a bed of chemical looping agent, direct heterogeneous reaction can allow the methane to be consumed if the solid is sufficiently active (e.g. iron oxide tends not to interact, whilst nickel oxide is very effective for the conversion of methane [51]). The oxygen carrier must not only be capable of providing oxygen, but also of showing some catalytic affinity for the conversion of methane.

Here, no combustion of methane with gaseous O_2 in FB rig was detected up to 700°C, with SiO_2 as bed material ($\sim 2.6\%CH_4/1.9\%O_2$ in N_2, ESI S.13). However, when $SrFeO_{3-\delta}$ was used as the bed material, it combusted methane mixture starting at 550°C (no O_2 was provided with the fluidizing gas). Gas profiles obtained during the experiments at 550 and 700°C are presented in Fig. 12. At low temperature a long-lasting oxygen release from the perovskite was observed, accompanied by slow but stable combustion of CH_4; no CO was detected and combustion was complete. At higher temperatures the rate of reaction increased but the gas phase oxygen was still present, clearly not all being consumed by the fuel.

For the combustion over a catalysts two possible reaction pathways can be discussed [52]: suprafacial, where oxygen and fuel molecule are both adsorbed on the catalyst surface; and intrafacial, where oxygen comes directly from the solid lattice. Perovskites can support both

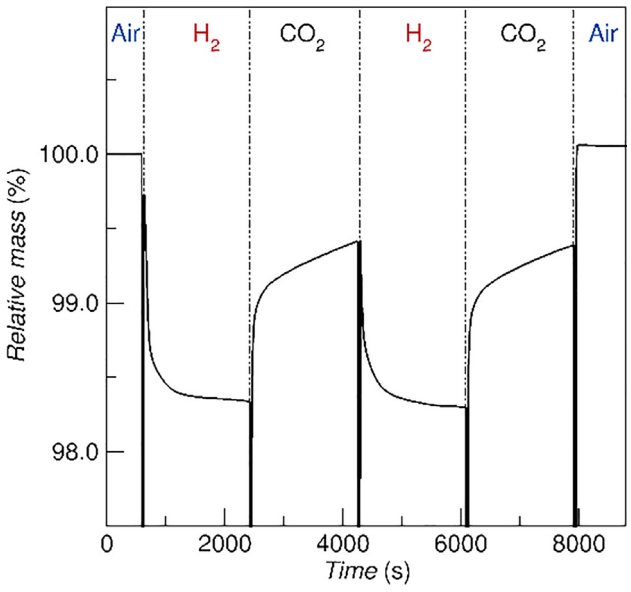

Fig. 9. Comparison of oxidation with CO_2 and air at 850°C. Isothermal program with reduction in H_2 and reoxidation with CO_2 or CO_2 followed by air. A 30 s. N_2 purge was introduced between gas switching. 100% for relative mass corresponds to the stable mass in air at 850°C.

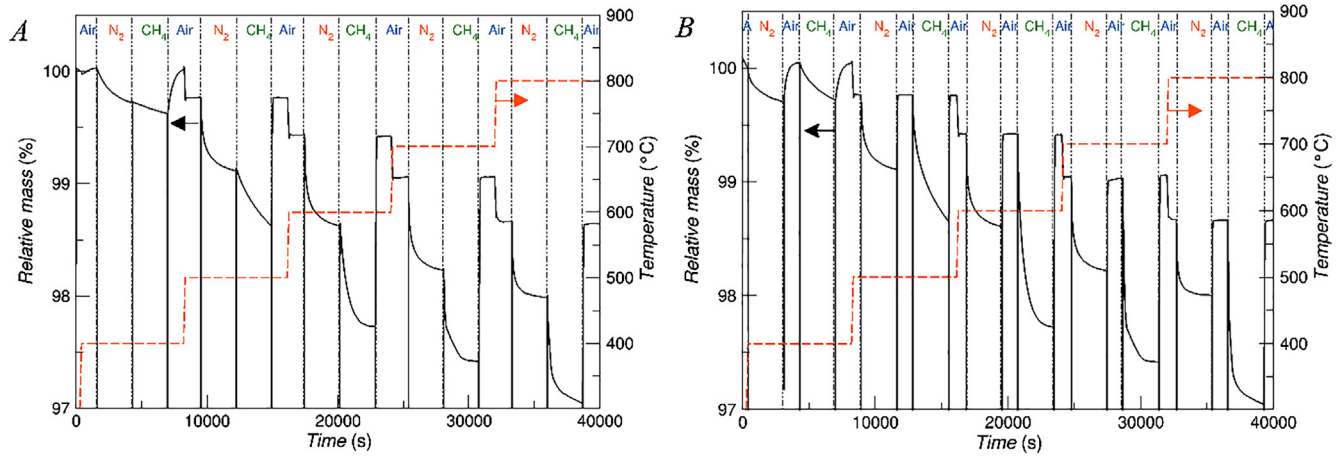

Fig. 10. TGA experiment for 5 isothermal steps carried at 400–800°C in: (a) 45 min N_2, 45 min CH_4, 20 min air, heat up in air, (b) 45 min N_2, 20 min air, 45 min CH_4, heat up in air.

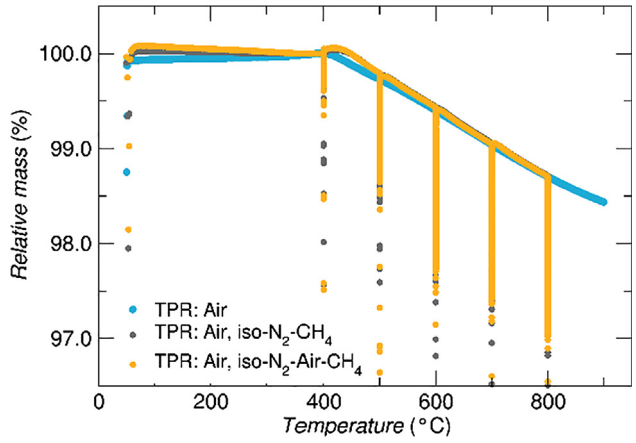

Fig. 11. Sample mass vs temperature in TPR in air and 5-step TPR-isothermal programs. In TPR-isothermal tests, the isothermal stages involved gas switching sequence: N_2, CH_4, air or N_2, air, CH_4, air (also Fig. 10 in the manuscript). In reoxidation at the end of each isothermals stage the sample mass got back to the same value as observed at the beginning of the isothermal step. Mass loss visible in the graph was due to temperature ramp up between each isothermal steps.

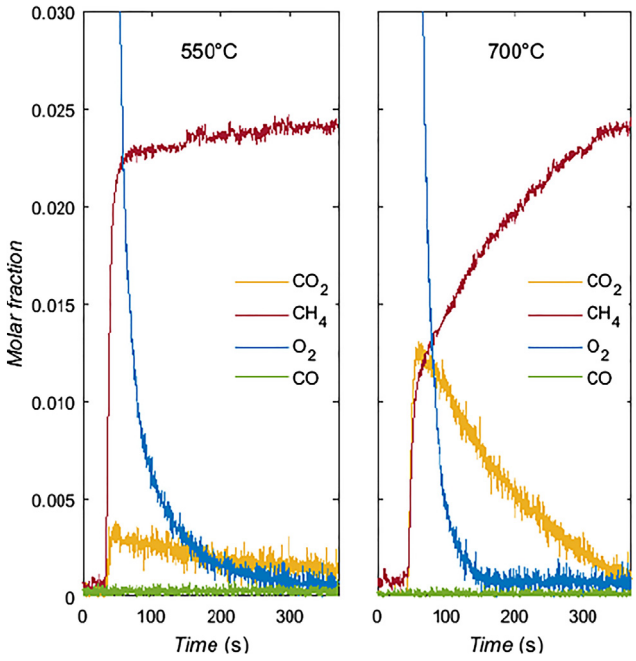

Fig. 12. Gas profiles during low concentration CH_4 combustion in fluidized bed rig at: 550°C, where oxygen release and low rate CH_4 combustion were observed; and at 700°C, where O_2 release and much faster CH_4 combustion were noticed. $SrFeO_{3-\delta}$ (15 g) was used as the bed material.

mechanisms in CH_4 combustion [53]. The suprafacial pathway can be expected at low temperatures, where O_2 adsorption on the surface is favourable. In the low temperature FB experiments (up to 500°C) with 15 g of $SrFeO_{3-\delta}$ no pronounced sign of CH_4 combustion was observed, despite the presence of released gaseous O_2. Under these conditions $SrFeO_{3-\delta}$ did not show catalytic activity, therefore neither possible pathway was active. On the contrary, the perovskite material assisted with methane combustion at higher temperatures, Fig. 12 ($T > 550$°C). As CH_4 was combusted, excess gaseous oxygen was also released from the perovskite. In this case, it is difficult to distinguish which catalytic mechanism dominates since $SrFeO_{3-\delta}$ uncouples oxygen at low temperatures at which CH_4 combustion would require a catalyst.

The CH_4 oxidation experiment proved that lean CH_4 combustion with $SrFeO_{3-\delta}$ is possible with an onset temperature (550°C) only slightly higher than temperatures for fluidized bed methane combustion carried out over metal catalysts ($T > 450$°C with Pd/Al_2O_3 catalyst [54]; $T > 650$°C with Cu/Al_2O_3 [55]). It is worth noticing that this type of materials catalysed CH_4 reaction with oxygen from air (continuously fed to reactor), opposite to $SrFeO_{3-\delta}$ being a source of oxygen itself. Moreover, the micro-structure of the investigated $SrFeO_{3-\delta}$ sample is very well developed, as can be seen in the SEM picture (ESI S.2). This may positively influence the catalytic properties of the material for the heterogeneous reactions.

Combustion over $SrFeO_{3-\delta}$ can be an interesting option for utilization of low CH_4 concentration mixtures, whilst avoiding the need for a noble metal catalyst to be present.

3.4.2. Multistep redox cycling with CO as the fuel

Typical gas profiles measured during 3-step redox cycling in the fluidized bed rig are shown in Fig. 13. Immediately before the experiment a blank experiment was performed. The sample was then dropped into the bed during the reduction phase of the first cycle, resulting in the production of oxygen and consumption of carbon monoxide. In the following cycles, reduction resulted in carbon dioxide production only. In the first oxidation step (with CO_2) carbon monoxide was the main product, in the second oxidation step oxygen was consumed. Altogether 30 redox cycles per experiment were performed. The measurements of gas concentrations were used to calculate the relative mass change of $SrFeO_{3-\delta}$, $m_r(-)$. Using CO_2 (reduction) or CO (1st oxidation) molar fractions:

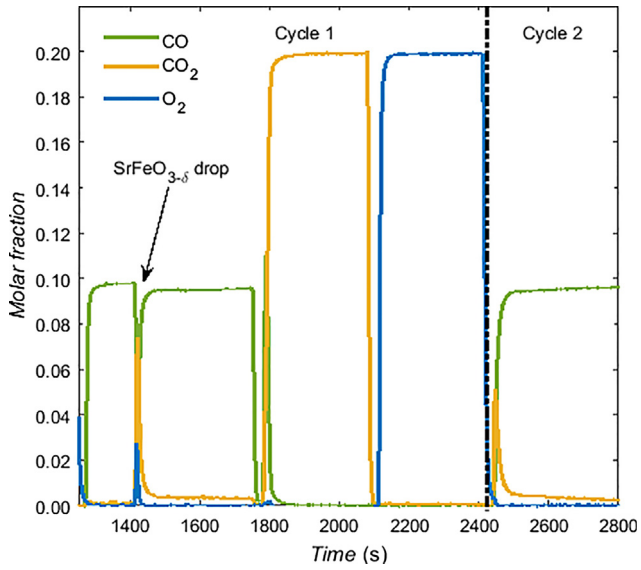

Fig. 13. Gas profiles during $SrFeO_{3-\delta}$ three step redox cycling in FB rig: 8 min reduction in 10% CO/N_2, 5 min oxidation in 20% CO_2/N_2, 5 min oxidation in air, between each stage: 0.5 min purge with N_2. Gas concentrations obtained during first and second cycle, T = 850°C.

$$m_r = M_O \cdot \int_{t_s}^{t_e} (x_{exp} - x_{blank}) \dot{V}_{FR}\ C_{total}\ dt / m_0 \quad (5)$$

Using O_2 (2nd oxidation) molar fractions:

$$m_r = M_{O_2} \cdot \int_{t_s}^{t_e} (x_{blank} - x_{exp}) \dot{V}_{FR}\ C_{total}\ dt / m_0 \quad (6)$$

where M_O, M_{O_2} is oxygen molar weight (16 or 32 g mol^{-1}), t_s and t_e represent time at the start and end of reduction or oxidation stage, x is the molar fraction of CO, CO_2 or O_2 measured in experiment and in a blank cycle (performed at the same temperature and flow conditions), $\dot{V}_{FR}$ is the gas flow rate at the reactor inlet (m^3/s), measured at ambient pressure and temperature: p = 101 325 Pa and T = 20°C, C_{total} is the total molar flow (mol/m^3), m_0 is the starting mass of the sample used in experiment (0.75 g). Additionally, since there was an O_2 release as the sample was added, the mass change calculations in the first cycle reduction step accounted for $m_{r_{O_2}}$ - the mass change connected with the O_2 peak: $m_r = m_{rCO} + m_{r_{O_2}}$, where $m_{r_{O_2}}$ was calculated in a similar way as presented in Eq. (5), but using M_{O_2} (32 g/mol) instead. No gas phase O_2 release was observed in the following cycles. In the calculation a diluted system with no change in the total molar flow was assumed.

The relative mass changes for the $SrFeO_{3-\delta}$ for the cycling experiments with reduction carried out in CO and the two-step oxidation (in CO_2, then in air) are shown in Fig. 14. The material showed good stability, with a similar conversion at each redox stage over the 30 cycles. The mass changes during the two stages of reduction totalled ~7%, which is higher than the mass loss in the experiments in the TGA. 7% represents material's total CLC capacity available at 850°C, i.e. the sum of oxygen released to the gas phase in a CLOU mechanism and oxygen removed from material via combustion with the reducing medium (CO). The sample tested in this experiment was retrieved from the reactor after last oxidation cycle, and was found to be $SrFeO_{3-\delta}$ (ESI S.8), showing that material regenerated back to a perovskite structure in the FB tests. The reduction in CO seemed to be reversed almost completely by the first oxidation carried out with 20% CO_2/N_2 mixture, with the second stage of oxidation only increasing the mass of the $SrFeO_{3-\delta}$ by a further ~1%. This ~1% mass change is lost in the N_2 purge and indicates the material's CLOU potential. The ~5.5–6% mass change during re-oxidation with CO_2 (or equivalently reduction in CO) represents the capacity to produce CO or H_2 (if steam were used as the oxidant).

A 2-step redox experiment (air oxidation omitted) was also performed and the results of the observed mass change over 30 cycles are presented in Fig. 15. Again a very stable behaviour over many cycles was seen with the mass change during reduction with CO matching that gained during oxidation with 20% CO_2. The final oxidation with air does not appear to be required to maintain stability, perhaps because CO_2 is sufficiently oxidizing to regenerate the perovskite phase.

Finally, Fig. 16 shows an experiment performed with 5% CO/10% CO_2 mixture as the reducing gas. The lower reducing potential of that mixture resulted in 1/3 of the reduction observed in tests with 10% CO (comparison of CO_2 production curves from both experiments is presented in ESI S.14). It is also clear from Fig. 16 that the reoxidation in 20% CO_2 after the reduction in 5% CO/10% CO_2 was not as efficient as in previous experiments.

The final air oxidation is crucial to maintain the material's activity in the next cycle. Specifically, if the second oxidation step under air is omitted, the mass change during reduction quickly decreases with cycle number (Fig. 16). Introduction of air in later cycles recovers some performance, but not to the level observed in the first cycles.

Finally, we note the reduction performance under N_2 displays considerable scatter (Fig. 16), though no clear trend emerges. The raw experimental concentration profiles can be seen in ESI S.15. To compare the combustion performance in all FB experiments, CO_2 production curves in reference to time are shown in ESI S.14. We noticed that combustion was the fastest and noticeable for the longest period of time when reducing gas did not contain CO_2. On contrary, the reaction in 5%CO/10%CO_2 atmosphere seemed to be suppressed by the presence of CO_2.

4. Discussion

For combustion application perovskites are often found to have low oxygen capacities. The stoichiometry of $SrFeO_3$ suggests that 4.18 wt% oxygen is available, but the practical capacity is lower due to inevitable oxygen nonstiochiometry (δ), if sample was not synthesised under high p_{O2} [38]. In-situ XRD analysis, as well as experiments performed in TGA and FB reactor showed that the perovskite can be reduced further than brownmillerite, resulting in phase separation to Fe and SrO. The phase

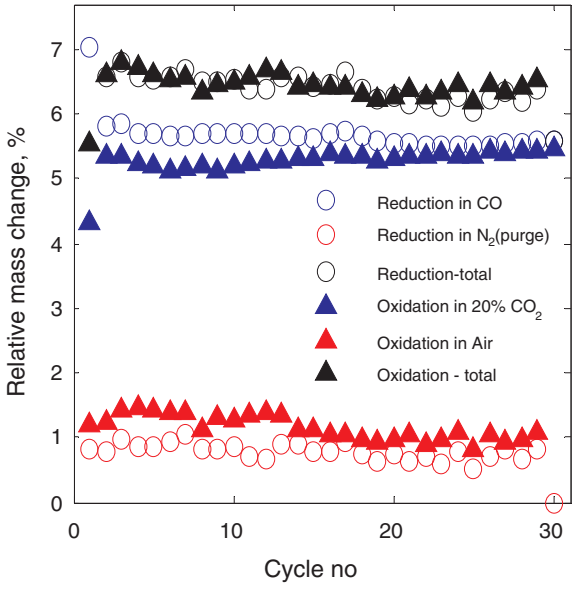

Fig. 14. $SrFeO_{3-\delta}$ sample mass loss due to redox stages in fluidized bed rig experiments (T = 850°C). 3-step cycling experiment (reduction: CO, oxidation: CO_2, air). Raw data, presenting gas profiles measured during reduction in N_2 (red symbols) is presented in ESI S.15.

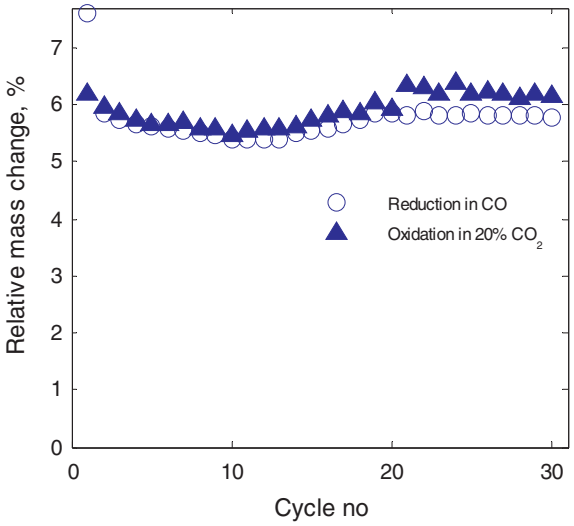

Fig. 15. $SrFeO_{3-\delta}$ sample mass loss due to redox stages in fluidized bed rig experiments (T = 850°C): 2-step cycling experiment (reduction: CO, oxidation: CO_2).

separation is completely reversible through oxidation in air or CO_2. Up to 7% of the material's mass change in fluidized bed experiments (850°C) represents total $SrFeO_{3-\delta}$ CLC capacity (O_2 availability for combustion), including ~1% of CLOU capacity (O_2 released to the gas phase), a > 50% higher oxygen capacity than the amount of O_2 calculated for the perovskite ($\delta = 0$)–brownmillerite ($\delta = 0.5$) phase change only. The ~1% CLOU capacity indicated that the material was able to re-oxidise to $SrFeO_{2.62}$ ($\delta = 0.38$) at these temperatures in air, and was probably limited by thermodynamic equilibrium. This is in good agreement with $SrFeO_{3-\delta}$ stoichiometry at $p_{O2} = 0.21$, 850°C presented in [15,42].

No problems due to particle sintering or attrition were encountered in the experiments (ESI S.16), the material can still be a potential option for the combustion. Nevertheless, longer term trials and more research is needed to investigate the vulnerability of $SrFeO_{3-\delta}$ to poisoning, e.g. by other flue-gas components such as oxides of sulphur or nitrogen.

In case of combustion applications another aspect that needs to be considered is the thermodynamic limitations imposed by the presence of combustion products: H_2O and CO_2. The TPR program that was performed in various CO/CO_2 atmospheres (Fig. 7B) showed that the introduction of CO_2 delays the combustion (starts at higher temperature than in CO) and limits the oxygen capacity available in the reduction. A similar effect can be observed during reduction of Fe_2O_3 in a fluidized bed reactor, where it is foreseen that due to the high p_{CO2} the only transition possible will be the reduction from hematite to magnetite [56]. Therefore in FB systems with Fe_2O_3 as a carrier, only about 11% of its oxygen capacity will be of use. On the other hand Bayham et al. calculated that an analogous system with a counter-current flows will allow to increase the utility of Fe-carrier to 50% of its capacity [3,56]. A reducer with a counter-current design have been developed by the group of Fan with a 25kWth CLC rig [57]. Hence, thermodynamic constrains for solid oxides reduction may not be an ultimate obstacle for applicability in chemical looping combustion. Similar systems with compounds such as $SrFeO_{3-\delta}$, which release oxygen into the gas phase, will allow for both high oxygen carrier and fuel conversion. Following the results from the TGA experiments (Fig. 7B) it can be concluded that relatively high p_{O2} simulated with $CO:CO_2$ mixture in 1:8 ratio (equivalent $p_{O2} = \sim 10^{-15}$ bar) allows for reduction that results in a mass loss of 2.5%, similar to the mass loss in hematite to magnetite reduction (3%). Relieving the thermodynamic constrains by a decrease of the effective p_{O2} in the reducer reactor will increase the potential available in $SrFeO_{3-\delta}$, ideally to ~7% mass change, as observed in FB

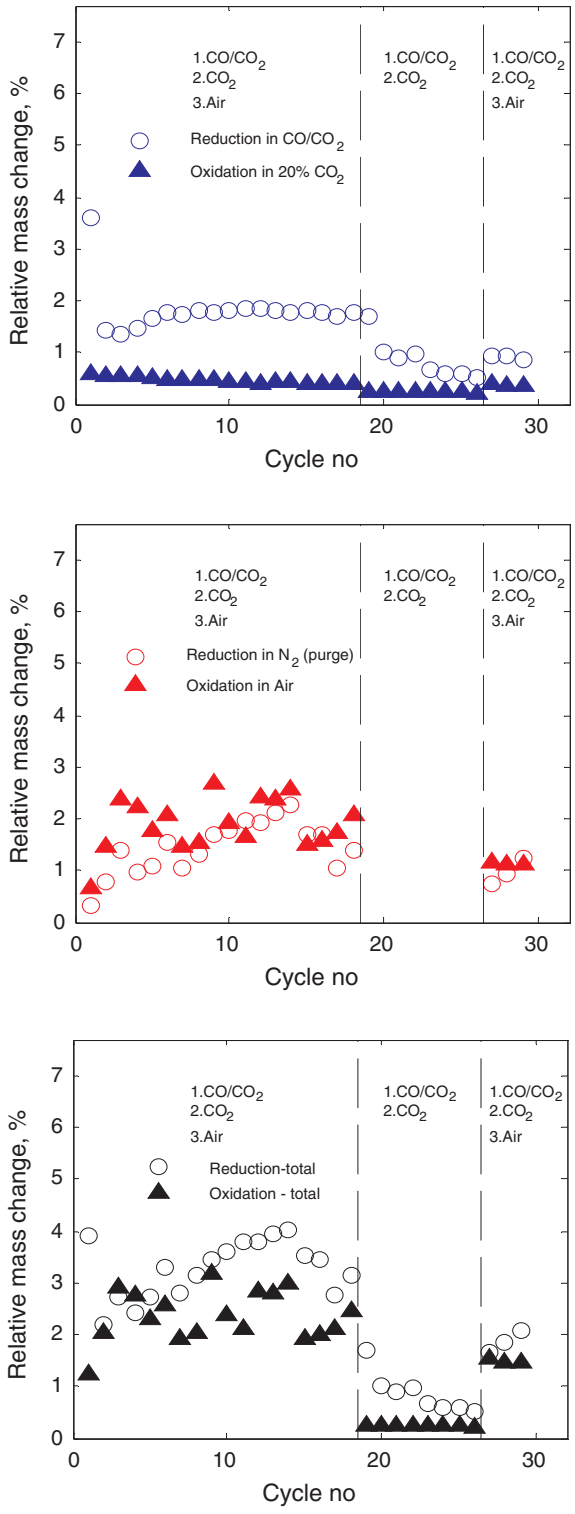

Fig. 16. $SrFeO_{3-\delta}$ sample mass loss due to redox stages in fluidized bed rig experiments (T = 850°C): 18 cycles in a 3-step cycling mode (reduction: CO/CO_2, oxidation: CO_2, air), followed by 8 cycles in a 2-step cycling mode (reduction: CO/CO_2, oxidation: CO_2), followed by 3 last cycles in a 3-step cycling mode (reduction: CO/CO_2, oxidation: CO_2, air). Raw data, presenting gas profiles measured during reduction in N_2 (red symbols) is presented in ESI S.15. (For interpretation of the references to colour in this figure legend, the reader is referred to the web version of this article.)

experiments. This, assuming that the starting material is $SrFeO_{2.82}$ and the final product is SrO + Fe, will represent usage of 45.5% of material's theoretical oxygen capacity.

Carbonation of $SrFeO_{3-\delta}$ is an interesting aspect that needs further investigations. As shown in Fig. 14, in FB rig during the reduction in CO up to 6% of the material mass was utilised in the combustion. Such a deep reduction did not result in coking or carbonation of the material (ESI S.17). Also no carbonation was observed during in-situ XRD experiments with CO_2 used for SrO + Fe reoxidation. On the other hand the TGA experiments with CO/CO_2 mixtures indicated a transient carbonation that was reversed as the temperature was increased (Fig. 7C)).

No carbonation was seen for pure $SrFeO_{3-\delta}$ perovskite in other studies [29]; they associated carbonation with the presence of impurities – namely the $Sr_3Fe_2O_7$ phase, and observed that carbonation of the impurities happened at higher temperatures and was not reversible. In our study, with higher purity samples, the material carbonated mostly at lower temperature and a TPO program was efficient to regenerate the sample. On the other hand Schmidt has shown that $SrFeO_{2.5}$, of brownmillerite structure, expected during 400–850°C part of the TPR program [15,45], is also prone to carbonation [41]. The $SrFeO_{2.5}$ carbonation was shown to start at temperature around 400°C (and was limited by slow reaction kinetics) but it was reversible at 870°C. The author suggests that the products of carbonation convert back to $SrFeO_x$ above a critical temperature that depends on CO_2 partial pressure and decreases with decreasing p_{CO2}. The TPR programs carried out in TGA with CO/CO_2 atmospheres indicate that indeed the carbonation was most likely connected to the brownmillerite phase (Fig. 8). In a more reducing atmosphere, with CO/CO_2 ratio 1:2 ($p_{CO2} \sim 0.03$ bar), the material reduced quickly resulting in a high share of the brownmillerite phase in the appropriate temperature window, which may have made the material susceptible to carbonation at intermediate temperatures. When the temperature was increased the mass gain due to carbonation was lost as the carbonates were likely reconverted to perovskite $SrFeO_x$. Moreover when the sample was reoxidized in air the mass returned to the starting value (if carbonates had not decomposed, the sample mass would have been higher). On the other hand, a higher share of CO_2 in the mixture (CO:CO_2 with a ratio 1:8, $p_{CO2} \sim 0.04$ bar) decreased the rate of material reduction. The slower reduction resulted in less brownmillerite being formed within the temperature window for carbonation, despite having a slightly higher p_{CO2}. Finally, after the very deep conversion in H_2, material did not seem to carbonate during reoxidation in CO_2. According to results by Grenier at al [39], at 850°C all brownmillerite should transition back to the cubic perovskite. Therefore it can be assumed that no brownmillerite was present and so sample was not prone to carbonation.

The transient character of carbonation is connected to the thermodynamic parameters (T and p_{CO2}, degree of material's reduction), and may also explain why no carbonation was visible in FB experiments in 10% CO reduction, despite the presence of CO_2 (measured up to 5% CO_2 concentration at the reactor outlet, Fig. 14). On the other hand, in experiments with twice as high CO_2 introduced directly to the FB reactor (5%CO/10%CO_2 mixture, Fig. 16), a small CO_2 release was observed during the reoxidation in air (ESI S.18, CO_2 peak up to 0.6%), indicating carbonation. Coking is a less plausible explanation since any coke would have been gasified during the 20% CO_2 oxidation stage. It is most likely that the material carbonated during the reduction stage. If it was only reduced and not carbonated then reoxidation with 20% CO_2 should be associated with a similar mass change during reduction, i.e. as in the experiment with reduction in 10% CO (Figs. 14 and 15). Instead, reoxidation with CO_2 was much less efficient as it was possibly obstructed by the presence of carbonates. Finally during the last stage, when air, with its low p_{co2} was introduced, decarbonation and oxidation could occur concurrently. When air-oxidation step was omitted in the second part of experiment presented in Fig. 16 with the cycle shortened to reduction in CO/CO_2 and CO_2 oxidation only, the material's activity quickly declined. As carbonated oxygen carrier could not regenerate in CO_2, it could not be reduced further either.

The fact that $SrFeO_{3-\delta}$ can be easily synthesised from $SrCO_3$ (3.1), and that carbonation only seems to occur over a narrow range of high p_{CO2} and under strongly reducing conditions (owing to the stability of the perovskite phase in the TGA), explains why the reversed reaction of carbonation should be expected, on reoxidation with air but perhaps not CO_2. Therefore, should a degradation in performance be observed, it may be possible to regenerate the material easily. On the other hand, the lack of carbonation in TGA when severely reduced sample was exposed to CO_2 at 900°C indicates that the carbonation can be avoided entirely when redox is carried out at higher temperatures (> 850°C).

Carbonation may not be as problematic in hydrogen production (H_2/H_2O systems), where material will be only in contact with CO_2 generated during the reduction step. Nevertheless both results from TGA as well as from FB experiments shown that a high partial pressure of a mild oxidizing gas, such as CO_2 in our study, or H_2O in hydrogen production, will influence the reduction process, imposing thermodynamic restrictions. Clearly, in order to evaluate the extent of that influence, a set of reliable thermodynamic data for $SrFeO_{3-\delta}$ is needed. To the authors' knowledge only limited information on $SrFeO_{3-\delta}$ phase diagram can be found in the literature. The most complete ones (in respect to T, p_{O2} and δ) were published by Mizusaki et al. [15] and Starkov et al. [42]. However, those works were limited to relatively high oxygen partial pressures only ($p_{O2} > 10^{-5}$ bar, eq. $CO_2/CO = 1.26 \cdot 10^6$ at 1123 K), characteristic for the spontaneous O_2 release stage, as observed e.g. during TPR in air or CO_2 shown in Fig. 7. To understand the reduction behaviour observed with H_2 or CO, a further investigation of possible phase transitions accompanying $SrFeO_{3-\delta}$ reduction to Fe and SrO, and their associated oxygen fugacity is needed. Nevertheless our study shows that $SrFeO_{3-\delta}$ is a very interesting material, also for the hydrogen production as the reoxidation with CO_2 was shown feasible.

It is worth noting that $SrFeO_{3-\delta}$ at its highest capacity during reoxidation in CO_2 (1 stage reoxidation only), resulted in a production of 3.75 $mmol_{CO}/g_{SrFeO3-\delta}$ and the same number can be expected for H_2 production when steam is used instead. That number was only about a half of H_2 yields that can be achieved with very stable Fe-Ca-Al carriers designed for H_2 production [58]. Nevertheless it is worth highlighting that $SrFeO_{3-\delta}$ showed very good cycling performance even without an intermediate reoxidation stage, and unlike Fe-Ca-Al materials, $SrFeO_{3-\delta}$ has the ability to produce gas phase oxygen during the first stage of reduction. It is also worth pointing out that the simple production method and low cost of both substrates ($SrCO_3$ and Fe_2O_3 are priced similarly at 1 tonne scale for materials of 97% purity) put the proposed $SrFeO_{3-\delta}$ perovskite in the range of the cheapest synthetic oxygen carriers, such as Fe_2O_3 by itself.

Chemical looping concepts present a promising approach for power generation combined with CO_2 capture. The attractiveness of this technology depends significantly on the extent to which the looping process can be integrated with the rest of the process flow sheet, e.g. the steam power cycle if used for power generation. As analysed by Khan and Shamim [59], the energy penalty connected to chemical looping combustion correlates with thermodynamic properties of the oxygen carrier and its oxygen transfer capacity. In addition to the thermodynamic constraints (supplying oxygen at the right chemical potential, and heat at the right temperature) and the capacity, cost and durability are also important. The capacity per mass is lower for perovskites than for monometallic carriers, requiring a higher circulation of solids.

As mentioned above, the cost of the raw materials for $SrFeO_{3-\delta}$ is relatively low, but the material is still manufactured and may not be as cost competitive as minerals that have been suggested for CLC [60]. The higher cost can be compensated for by a longer lifetime; dictated by chemical and mechanical stability. In the present work, the losses in material activity through interaction with impurities or attrition were minor, but the chemical and mechanical stresses experienced in lab tests are of different magnitude and duration to those in a full scale circulating system. Chemical looping combustion is not overly restricted by material thermodynamics, providing material can release or donate oxygen at the required temperature range (i.e. T > 850°C for

fluidized bed coal CLC), making integration with the power cycle straight forward. Accordingly, the cost is primarily driven by the makeup rate and the cost per mass of the oxygen carrier, and thus cheap minerals are a difficult benchmark to beat. Further work is needed to establish if $SrFeO_{3-\delta}$ would have a lifetime sufficient to compete with the mineral carriers. Moreover, the study tested the material in the operating temperature up to 900°C. This allows to conclude about $SrFeO_{3-\delta}$ potential and feasibility for integration in coal combustion units. For coal gasification plants (iGCLC), where turbine inlet temperature will be in a range of 1300°C [61,62], the lower temperatures required in the redox loops will impose thermal and therefore efficiency losses.

For other processes which do require the oxygen chemical potential to be optimised, the potential advantages of $SrFeO_{3-\delta}$ are more clear. In these processes, the mechanical stresses may be lowered by using packed beds, and the chemical environment is more carefully controlled. For example, systems can be designed such that the oxygen carrier does not come into contact with ash, or in some cases even the fuel. So far, $SrFeO_{3-\delta}$ has been recognized as a promising material for oxygen production integrated with coal oxy-fuel combustion (CLAS-oxy-fuel) [63] using the transition between $SrFeO_{3-\delta}$ and $SrFeO_{2.5}$ (identified for O_2 production). Given the limited structural change, a material might be expect to cycle indefinably. Our work shows that the transition between $SrFeO_{2.5}$ and Fe + SrO has a large oxygen capacity, and chemical potential very suited also to hydrogen production. Further flow sheeting studies are needed to establish if the promising thermodynamic properties translate into a competitive efficiency when the process is fully integrated.

5. Conclusions

This study demonstrates that solid synthesis with $SrCO_3$ and Fe_2O_3 is a simple and efficient preparation method that results in production of pure $SrFeO_{3-\delta}$ in a perovskite structure. The material can catalytically assist with combustion of lean CH_4 (2.5%) in fluidized bed, at temperatures > 550°C. Long $SrFeO_{3-\delta}$ reductions, carried out with highly reducing atmospheres in TGA and fluidized bed reactor, accounted for more than 4.18% mass change, indicating reduction below $\delta = 0.5$. This report shows that much deeper reduction, from $SrFeO_{3-\delta}$ to SrO and Fe, is reversible and results in oxygen release at a chemical potential suitable for hydrogen production. This was also confirmed with in-situ XRD, where diffraction patterns clearly showed the final products of $SrFeO_{3-\delta}$ reduction were Fe and SrO. Moreover, the deeply reduced material can be partially regenerated to $SrFeO_{2.5}$ by oxidation in CO_2 or completely regenerated to $SrFeO_{3-\delta}$ in air.

The possibility of using a mild oxidant, such as CO_2 or H_2O, makes $SrFeO_{3-\delta}$ attractive for CO or H_2 production. The material was stable to repeated cycles of reduction in 10% CO, in terms of $SrFeO_{3-\delta}$ conversion (measured by mass change) and particle mechanical robustness (no sintering nor attrition was observed) during long cycling experiments in a fluidized bed reactor. There is a narrow window in which the material can carbonate (in high p_{CO2} and when the material is reduced), although carbonates can be removed by oxidation or avoided entirely by using higher temperatures (> 850°C).

Data

A set of all collected experimental and supporting data for this work can be found on https://www.repository.cam.ac.uk.

Acknowledgments

This research was carried out with the financial support from EPSRC grant no. EP/K030132/1. MWG is grateful for support from the European Union's Horizon 2020 research and innovation programme under the Marie Skłodowska–Curie grant agreement No. 659764.

Appendix A. Supplementary material

Supplementary data associated with this article can be found, in the online version, at http://dx.doi.org/10.1016/j.apenergy.2018.04.090.

References

[1] Meredig B, Wolverton C. First-principles thermodynamic framework for the evaluation of thermochemical H_2O- or CO_2-splitting materials. Phys Rev B 2009;80:245119. http://dx.doi.org/10.1103/PhysRevB.80.245119.
[2] Mattisson T, Adánez J, Mayer K, Snijkers F, Williams G, Wesker E, et al. Innovative oxygen carriers uplifting chemical-looping combustion. Energy Proc 2014;63:113–30. http://dx.doi.org/10.1016/j.egypro.2014.11.012.
[3] Bayham SC, Tong A, Kathe M, Fan L-S. Chemical looping technology for energy and chemical production: chemical looping technology. Wiley Interdiscip Rev Energy Environ 2016;5:216–41. http://dx.doi.org/10.1002/wene.173.
[4] Pour NM, Azimi G, Leion H, Rydén M, Lyngfelt A. Production and examination of oxygen-carrier materials based on manganese ores and $Ca(OH)_2$ in chemical looping with oxygen uncoupling. AIChE J 2014;60:645–56. http://dx.doi.org/10.1002/aic.14273.
[5] Lyngfelt A. Chemical-looping combustion of solid fuels – status of development. Appl Energy 2014;113:1869–73. http://dx.doi.org/10.1016/j.apenergy.2013.05.043.
[6] Siriwardane R, Benincosa W, Riley J, Tian H, Richards G. Investigation of reactions in a fluidized bed reactor during chemical looping combustion of coal/steam with copper oxide-iron oxide-alumina oxygen carrier. Appl Energy 2016;183:1550–64. http://dx.doi.org/10.1016/j.apenergy.2016.09.045.
[7] Akbari-Emadabadi S, Rahimpour MR, Hafizi A, Keshavarz P. Production of hydrogen-rich syngas using Zr modified Ca-Co bifunctional catalyst-sorbent in chemical looping steam methane reforming. Appl Energy 2017;206:51–62. http://dx.doi.org/10.1016/j.apenergy.2017.08.174.
[8] Sun Z, Lu DY, Ridha FN, Hughes RW, Filippou D. Enhanced performance of ilmenite modified by CeO_2, ZrO_2, NiO, and Mn_2O_3 as oxygen carriers in chemical looping combustion. Appl Energy 2017;195:303–15. http://dx.doi.org/10.1016/j.apenergy.2017.03.014.
[9] Imtiaz Q, Hosseini D, Müller CR. Review of oxygen carriers for chemical looping with oxygen uncoupling (CLOU): thermodynamics, material development, and synthesis. Energy Technol 2013;1:633–47. http://dx.doi.org/10.1002/ente.201300099.
[10] Luo S, Zeng L, Fan L-S. Chemical looping technology: oxygen carrier characteristics. Annu Rev Chem Biomol Eng 2015;6:53–75. http://dx.doi.org/10.1146/annurev-chembioeng-060713-040334.
[11] Thursfield A, Murugan A, Franca R, Metcalfe IS. Chemical looping and oxygen permeable ceramic membranes for hydrogen production – a review. Energy Environ Sci 2012;5:7421. http://dx.doi.org/10.1039/c2ee03470k.
[12] Voitic G, Hacker V. Recent advancements in chemical looping water splitting for the production of hydrogen. RSC Adv 2016;6:98267–96. http://dx.doi.org/10.1039/C6RA21180A.
[13] Reller A. Chemical and physical implications of cationic and anionic modifications in perovskite related metal oxides. Philos Mag A 1993;68:641–52. http://dx.doi.org/10.1080/01418619308213988.
[14] Vieten J, Bulfin B, Call F, Lange M, Schmücker M, Francke A, et al. Perovskite oxides for application in thermochemical air separation and oxygen storage. J Mater Chem A 2016;4:13652–9. http://dx.doi.org/10.1039/C6TA04867F.
[15] Mizusaki J, Okayasu M, Yamauchi S, Fueki K. Nonstoichiometry and phase relationship of the SrFeO2.5-SrFeO3 system at high temperature. J Solid State Chem 1992;99:166–72. http://doi.org/10.1016/0022-4596(92)90301-B.
[16] Ezbiri M, Allen KM, Gàlvez ME, Michalsky R, Steinfeld A. Design principles of perovskites for thermochemical oxygen separation. ChemSusChem 2015;8:1966–71. http://dx.doi.org/10.1002/cssc.201500239.
[17] Nalbandian L, Evdou A, Zaspalis V. $La_{1-x}Sr_xMO_3$ (M = Mn, Fe) perovskites as materials for thermochemical hydrogen production in conventional and membrane reactors. Int J Hydrog Energy 2009;34:7162–72. http://dx.doi.org/10.1016/j.ijhydene.2009.06.076.
[18] Arjmand M, Kooiman RF, Rydén M, Leion H, Mattisson T, Lyngfelt A. Sulfur tolerance of $Ca_xMn_{1-y}M_yO_{3-\delta}$ (M = Mg, Ti) perovskite-type oxygen carriers in chemical-looping with oxygen uncoupling (CLOU). Energy Fuels 2014;28:1312–24. http://dx.doi.org/10.1021/ef402383v.
[19] Lin Y-S, MacLean DL, Zeng Y. High temperature adsorption process. US6059858 A; 2000.
[20] Yang Z, Lin YS, Zeng Y. High-temperature sorption process for air separation and oxygen removal. Ind Eng Chem Res 2002;41:2775–84. http://dx.doi.org/10.1021/ie010736k.
[21] Galinsky NL. Investigation of redox metal oxides for carbonaceous fuel conversion and CO2 capture. North Carolina State University; 2016.
[22] Evdou A, Zaspalis V, Nalbandian L. $La_{1-x}Sr_xFeO_{3-\delta}$ perovskites as redox materials for application in a membrane reactor for simultaneous production of pure hydrogen and synthesis gas. Fuel 2010;89:1265–73. http://dx.doi.org/10.1016/j.fuel.2009.09.028.
[23] Emery AA, Saal JE, Kirklin S, Hegde VI, Wolverton C. High-throughput computational screening of perovskites for thermochemical water splitting applications. Chem Mater 2016;28:5621–34. http://dx.doi.org/10.1021/acs.chemmater.6b01182.
[24] Jun A, Kim J, Shin J, Kim G. Perovskite as a cathode material: a review of its role in

solid-oxide fuel cell technology. ChemElectroChem 2016;3:511–30. http://dx.doi.org/10.1002/celc.201500382.
[25] Kilner JA, Burriel M. Materials for intermediate-temperature solid-oxide fuel cells. Annu Rev Mater Res 2014;44:365–93. http://dx.doi.org/10.1146/annurev-matsci-070813-113426.
[26] Gallucci F, Fernandez E, Corengia P, van Sint Annaland M. Recent advances on membranes and membrane reactors for hydrogen production. Chem Eng Sci 2013;92:40–66. http://dx.doi.org/10.1016/j.ces.2013.01.008.
[27] Li Y, Rui Z, Xia C, Anderson M, Lin YS. Performance of ionic-conducting ceramic/carbonate composite material as solid oxide fuel cell electrolyte and CO_2 permeation membrane. Catal Today 2009;148:303–9. http://dx.doi.org/10.1016/j.cattod.2009.08.009.
[28] Dunstan MT, Liu W, Pavan AF, Kimpton JA, Ling CD, Scott SA, et al. Reversible CO_2 absorption by the 6H perovskite $Ba_4Sb_2O_9$. Chem Mater 2013;25:4881–91. http://dx.doi.org/10.1021/cm402875v.
[29] Lau CY, Dunstan MT, Hu W, Grey CP, Scott SA. Large scale in silico screening of materials for carbon capture through chemical looping. Energy Env Sci 2017. http://dx.doi.org/10.1039/C6EE02763F.
[30] Mihai O, Chen D, Holmen A. Catalytic consequence of oxygen of lanthanum ferrite perovskite in chemical looping reforming of methane. Ind Eng Chem Res 2011;50:2613–21. http://dx.doi.org/10.1021/ie100651d.
[31] Yin Q, Kniep J, Lin YS. Oxygen sorption and desorption properties of Sr–Co–Fe oxide. Chem Eng Sci 2008;63:2211–8. http://dx.doi.org/10.1016/j.ces.2008.01.016.
[32] Evdou A, Zaspalis V, Nalbandian L. $La_{(1-x)}Sr_xMnO_{3-\delta}$ perovskites as redox materials for the production of high purity hydrogen. Int J Hydrog Energy 2008;33:5554–62. http://dx.doi.org/10.1016/j.ijhydene.2008.06.036.
[33] Dueso C, Thompson C, Metcalfe I. High-stability, high-capacity oxygen carriers: Iron oxide-perovskite composite materials for hydrogen production by chemical looping. Appl Energy 2015;157:382–90. http://dx.doi.org/10.1016/j.apenergy.2015.05.062.
[34] Zhao K, He F, Huang Z, Zheng A, Li H, Zhao Z. Three-dimensionally ordered macroporous $LaFeO_3$ perovskites for chemical-looping steam reforming of methane. Int J Hydrog Energy 2014;39:3243–52. http://dx.doi.org/10.1016/j.ijhydene.2013.12.046.
[35] Zhao K, He F, Huang Z, Wei G, Zheng A, Li H, et al. Perovskite-type oxides $LaFe_{1-x}Co_xO_3$ for chemical looping steam methane reforming to syngas and hydrogen co-production. Appl Energy 2016;168:193–203. http://dx.doi.org/10.1016/j.apenergy.2016.01.052.
[36] Zhao K, Li L, Zheng A, Huang Z, He F, Shen Y, et al. Synergistic improvements in stability and performance of the double perovskite-type oxides $La_{2-x}Sr_xFeCoO_6$ for chemical looping steam methane reforming. Appl Energy 2017;197:393–404. http://dx.doi.org/10.1016/j.apenergy.2017.04.049.
[37] Coelho A. TOPAS academic, V5 Coelho Software. Brisbane, Australia: Coelho Software; 2013.
[38] Dann SE, Currie DB, Weller MT, Thomas MF, Al-Rawwas AD. The Effect of oxygen stoichiometry on phase relations and structure in the system La21-xSrxFeO3-δ ($0 \leq x \leq 1$, $0 \leq \delta \leq 0.5$). J Solid State Chem 1994;109:134–44. http://doi.org/10.1006/jssc.1994.1083.
[39] Grenier J-C, Ea N, Pouchard M, Hagenmuller P. Structural transitions at high temperature in $Sr_2Fe_{2O}5$. J Solid State Chem 1985;58:243–52. http://dx.doi.org/10.1016/0022-4596(85)90241-5.
[40] Savinskaya OA, Nemudry AP, Nadeev AN, Tsybulya SV. Synthesis and study of the thermal stability of $SrFe_{1-x}M_xO_{3-z}$ (M = Mo, W) perovskites. Solid State Ion 2008;179:1076–9. http://dx.doi.org/10.1016/j.ssi.2008.02.005.
[41] Schmidt M. Mechanical and thermal carbonation of strontium ferrite $SrFeO_x$. Mater Res Bull 2002;37:2093–105. http://dx.doi.org/10.1016/S0025-5408(02)00898-X.
[42] Starkov I, Bychkov S, Matvienko A, Nemudry A. Oxygen release technique as a method for the determination of " δ–p_{O2}–T " diagrams for MIEC oxides. Phys Chem Chem Phys 2014;16:5527–35. http://dx.doi.org/10.1039/C3CP52143E.
[43] Takeda Y, Kanno K, Takada T, Yamamoto O, Takano M, Nakayama N, et al. Phase relation in the oxygen nonstoichiometric system, SrFeOx ($2.5 \leq x \leq 3.0$). J Solid State Chem 1986;63:237–49. http://doi.org/10.1016/0022-4596(86)90174-X.
[44] Schmidt M, Campbell SJ. In situ neutron diffraction study (300–1273K) of non-stoichiometric strontium ferrite $SrFeO_x$. J Phys Chem Solids 2002;63:2085–92. http://dx.doi.org/10.1016/S0022-3697(02)00198-1.
[45] Taylor DD, Schreiber NJ, Levitas BD, Xu W, Whitfield PS, Rodriguez EE. Oxygen storage properties of $La_{1-x}Sr_xFeO_{3-\delta}$ for chemical-looping reactions—an in situ neutron and synchrotron X-ray study. Chem Mater 2016;28:3951–60. http://dx.doi.org/10.1021/acs.chemmater.6b01274.
[46] Fossdal A, Einarsrud M-A, Grande T. Phase equilibria in the pseudo-binary system SrO–Fe_2O_3. J Solid State Chem 2004;177:2933–42. http://dx.doi.org/10.1016/j.jssc.2004.05.007.
[47] Kleveland K, Einarsrud M-A, Grande T. sintering behavior, microstructure, and phase composition of $Sr(Fe, Co)_{O3-}\delta$ ceramics. J Am Ceram Soc 2000;83:3158–64. http://dx.doi.org/10.1111/j.1151-2916.2000.tb01698.x.
[48] Vieten J, Bulfin B, Senholdt M, Roeb M, Sattler C, Schmücker M. Redox thermodynamics and phase composition in the system $SrFeO_{3-\delta}$ — $SrMnO_{3-\delta}$. Solid State Ion 2017;308:149–55. http://dx.doi.org/10.1016/j.ssi.2017.06.014.
[49] Bucher E, Egger A, Caraman GB, Sitte W. Stability of the SOFC cathode material (Ba, Sr)(Co, $Fe_{)O3}$ − δ in $_cO2$-containing atmospheres. J Electrochem Soc 2008;155:B1218–24. http://dx.doi.org/10.1149/1.2981024.
[50] Hesketh RP, Davidson JF. Combustion of methane and propane in an incipiently fluidized bed. Combust Flame 1991;85:449–67. http://dx.doi.org/10.1016/0010-2180(91)90147-4.
[51] Johansson M, Mattisson T, Lyngfelt A. Creating a synergy effect by using mixed oxides of iron- and nickel oxides in the combustion of methane in a chemical-looping combustion reactor. Energy Fuels 2006;20:2399–407. http://dx.doi.org/10.1021/ef060068l.
[52] Peña MA, Fierro JLG. Chemical structures and performance of perovskite oxides. Chem Rev 2001;101:1981–2018. http://dx.doi.org/10.1021/cr980129f.
[53] Ladavos AK, Pomonis J. Catalytic combustion of methane on $La_{2-x}Sr_xNiO_{4-\lambda}$ (x = 0.00–1.50) perovskites prepared via the nitrate and citrate routes. J Chem Soc Faraday Trans 1992;88:2557–62. http://dx.doi.org/10.1039/FT9928802557.
[54] Yang Z, Yang P, Zhang L, Guo M, Yan Y. Investigation of low concentration methane combustion in a fluidized bed with Pd/Al_2O_3 as catalytic particles. RSC Adv 2014;4:59418–26. http://dx.doi.org/10.1039/C4RA08534E.
[55] Iamarino M, Ammendola P, Chirone R, Pirone R, Ruoppolo G, Russo G. Nonpremixed catalytic combustion of methane in a fluidized bed reactor. Ind Eng Chem Res 2006;45:1009–13. http://dx.doi.org/10.1021/ie051015e.
[56] Zeng L, Tong A, Kathe M, Bayham S, Fan L-S. Iron oxide looping for natural gas conversion in a countercurrent moving bed reactor. Appl Energy 2015;157:338–47. http://dx.doi.org/10.1016/j.apenergy.2015.06.029.
[57] Tong A, Bayham S, Kathe MV, Zeng L, Luo S, Fan L-S. Iron-based syngas chemical looping process and coal-direct chemical looping process development at Ohio State University. Appl Energy 2014;113:1836–45. http://dx.doi.org/10.1016/j.apenergy.2013.05.024.
[58] Ismail M, Liu W, Dunstan MT, Scott SA. Development and performance of iron based oxygen carriers containing calcium ferrites for chemical looping combustion and production of hydrogen. Int J Hydrog Energy 2016;41:4073–84. http://dx.doi.org/10.1016/j.ijhydene.2015.11.066.
[59] Khan MN, Shamim T. Thermodynamic screening of suitable oxygen carriers for a three reactor chemical looping reforming system. Int J Hydrog Energy 2017;42:15745–60. http://dx.doi.org/10.1016/j.ijhydene.2017.05.037.
[60] Lyngfelt A, Mattisson T, Rydén M, Linderholm CJ. Chemical-Looping combustion of solid fuels – what is needed to reach full-scale? In: 4th Int. Conf. Chem. Looping Sept. 26–28 Nanjing China; 2016.
[61] Adanez J, Abad A, Garcia-Labiano F, Gayan P, de Diego LF. Progress in chemical-looping combustion and reforming technologies. Prog Energy Combust Sci 2012;38:215–82. http://dx.doi.org/10.1016/j.pecs.2011.09.001.
[62] Mukherjee S, Kumar P, Yang A, Fennell P. Energy and exergy analysis of chemical looping combustion technology and comparison with pre-combustion and oxy-fuel combustion technologies for CO2 capture. J Environ Chem Eng 2015;3:2104–14. http://dx.doi.org/10.1016/j.jece.2015.07.018.
[63] Görke RH, Hu W, Dunstan MT, Dennis JS, Scott SA. Exploration of the material property space for chemical looping air separation applied to carbon capture and storage. Appl Energy 2018;212:478–88. http://dx.doi.org/10.1016/j.apenergy.2017.11.083.